Title

Glutamine Sensitivity Analysis Identifies the xCT Antiporter as a Common Triple-Negative Breast Tumor Therapeutic Target

Journal

Cancer Cell, 2013(24)

Authors

Timmerman, Luika A
Holton, Thomas
Yuneva, Mariia
et al.

Publication Date

2013-10-14

Peer reviewed

Cancer Cell
Article

Glutamine Sensitivity Analysis Identifies the xCT Antiporter as a Common Triple-Negative Breast Tumor Therapeutic Target

Luika A. Timmerman,[1,*] Thomas Holton,[4] Mariia Yuneva,[6] Raymond J. Louie,[1,3] Mercè Padró,[1,3] Anneleen Daemen,[1,2] Min Hu,[5] Denise A. Chan,[1,3] Stephen P. Ethier,[7] Laura J. van 't Veer,[1,2] Kornelia Polyak,[8] Frank McCormick,[1,10] and Joe W. Gray[9,10]

[1]UCSF/Helen Diller Family Comprehensive Cancer Center
[2]Department of Laboratory Medicine
[3]Department of Radiation Oncology
University of California, San Francisco, San Francisco, CA 94115, USA
[4]School of Engineering, San Francisco State University, San Francisco, CA 94115, USA
[5]Novartis Institutes for BioMedical Research (China), Pudong New Area, Shanghai 201203, P.R. China
[6]Division of Physiology and Metabolism, MRC National Institute of Medical Research, London NW7 1AA, UK
[7]Hollings Cancer Center, Medical University of South Carolina, Charleston, SC 29425, USA
[8]Department of Medical Oncology, Dana-Farber Cancer Institute, Harvard Medical School, Boston, MA 02215, USA
[9]Department of Biomedical Engineering, Oregon Health Sciences University, Portland, OR 97239, USA
[10]These authors contributed equally to this work
*Correspondence: timmerma@cc.ucsf.edu
http://dx.doi.org/10.1016/j.ccr.2013.08.020

SUMMARY

A handful of tumor-derived cell lines form the mainstay of cancer therapeutic development, yielding drugs with an impact typically measured as months to disease progression. To develop more effective breast cancer therapeutics and more readily understand their clinical impact, we constructed a functional metabolic portrait of 46 independently derived breast cell lines. Our analysis of glutamine uptake and dependence identified a subset of triple-negative samples that are glutamine auxotrophs. Ambient glutamine indirectly supports environmental cystine acquisition via the xCT antiporter, which is expressed on one-third of triple-negative tumors in vivo. xCT inhibition with the clinically approved anti-inflammatory sulfasalazine decreases tumor growth, revealing a therapeutic target in breast tumors of poorest prognosis and a lead compound for rapid, effective drug development.

INTRODUCTION

Current cancer therapeutic development methodologies are expensive, slow, and unable to allow early prediction of the palette and prevalence of responses tumors can mount when challenged with a prototypic drug. Breast cancer is a challenging example. Large heterogeneity exists within and between well-established subtypes and drug responses (reviewed in Weigelt and Reis-Filho, 2009). Three distinct nomenclatures group breast tumors based on morphological criteria (e.g., ductal, lobular, invasive, or in situ); expression of the estrogen receptor (ER), progesterone receptor (PR), and Her2 receptor tyrosine kinase (Her2); or molecular phenotype, derived from comprehensive mRNA similarities (e.g., luminal, basal). Approximately one-fourth of breast tumors are "triple negative" (ER^-/ PR^-/ $Her2^-$; TNBC), and usually have a basal molecular phenotype. They are aggressive, with poorest prognosis, high mitotic index, and intrinsic DNA damage repair defects (reviewed in Weigelt and Reis-Filho, 2009; Alli et al., 2009). A subset termed claudin low and related metaplastic tumors have rapid disease courses,

Significance

There is a strong disconnect between compound efficacy in tumor cell lines used for cancer drug development versus clinical response rates, slowing the production of effective therapeutics. This would be improved if the frequency and types of tumor responses to a particular perturbation could be identified early in the process. While drug target expression is currently used to identify applicable clinical populations, these patient cohorts contain both responders and nonresponders. Here, we use functional analyses in 47 independent breast-derived cell lines to measure metabolic responses related to perturbations in glutamine metabolism, and estimate their frequency. We identify a therapeutic target in a severely underserved population of patients with breast cancer and a lead compound for rapid, durable therapeutic development.

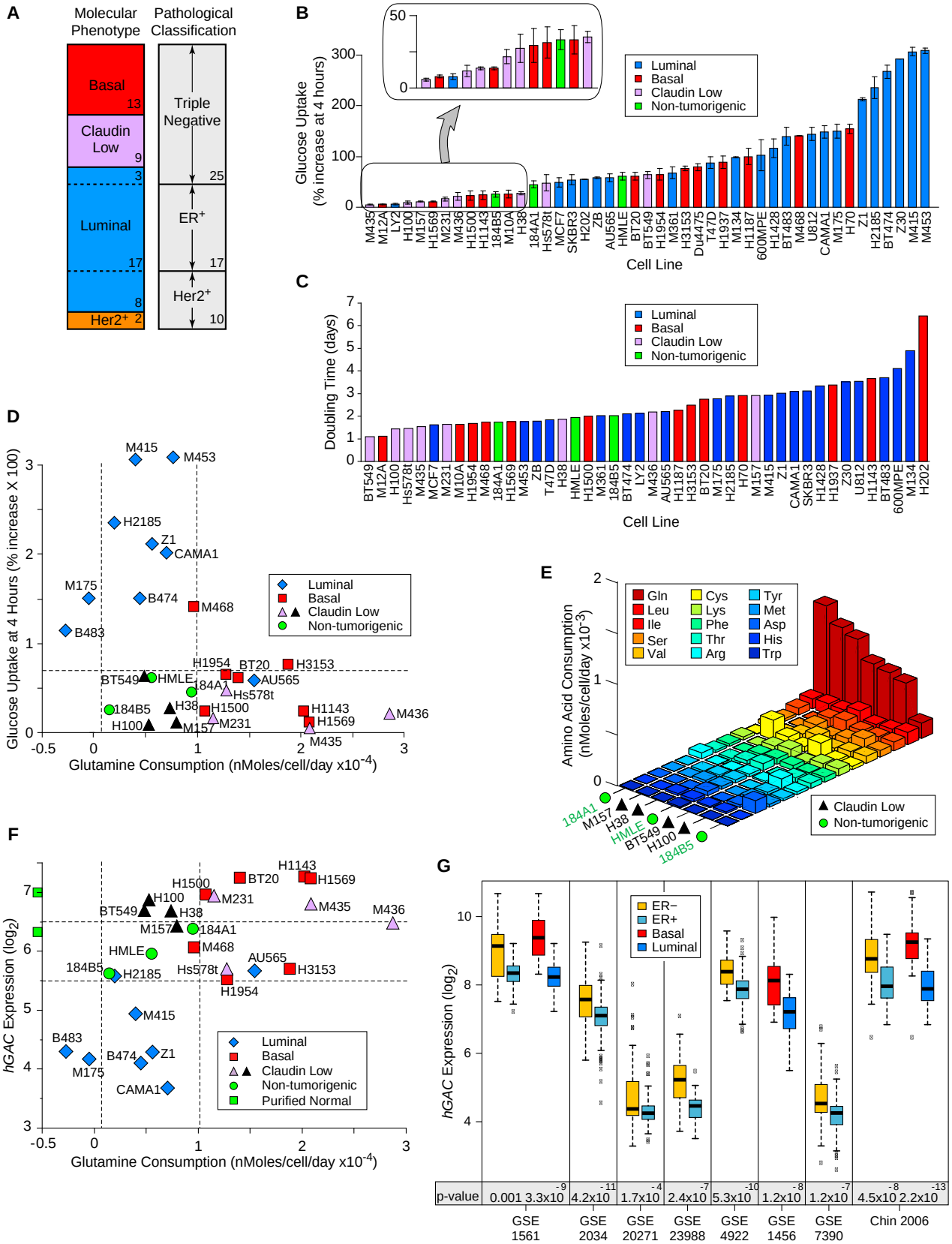

(legend on next page)

stem cell features, and chemotherapy-resistant characteristics (Hennessy et al., 2009, Prat et al., 2010). No TNBC-targeted therapeutic exists, and patient prognosis is grim.

Many tumors increase uptake and reliance on environmental nutrients such as glucose, glutamine (reviewed in Souba, 1993; Gatenby and Gillies, 2004; DeBerardinis et al., 2008), cystine, and asparagine (Iglehart et al., 1977; Asselin et al., 1989). Seminal work in tumor series of increasing proliferation rate and de-differentiation (Erlich ascites, Knox et al., 1970; Morris hepatoma, Linder-Horowitz et al., 1969; Nb2 lymphoma, Gout et al., 1997) correlated these features with malignant progression, fostering drug development efforts focused on specific nutrients. However, resulting nutrient mimetics were systemically toxic (reviewed in Souba, 1993), and inexplicable variability among increasing numbers of tumor isolates eventually discouraged these endeavors. Only leukemia dependence on asparagine was successfully pursued to a molecular understanding and effective drug (Asparaginase, reviewed in Narta et al., 2007).

The xCT cystine/glutamate antiporter is the major means of increasing cystine uptake and the rate-limiting step for glutathione (GSH) synthesis in fibroblasts, rat hepatocytes, and Nb2 lymphoma (Bannai and Tateishi, 1986; Gout et al., 1997). Dual roles in reactive oxygen species (ROS) neutralization and detoxification of xenobiotics such as chemotherapeutics make GSH an appealing drug target. However, inhibitors of glutathione synthesis failed clinical trials due to toxicities related to systemic GSH depletion (reviewed in Hamilton and Batist, 2004). xCT may provide a target for cell-specific GSH depletion. Drug screens identified off-target effects of the anti-inflammatory pro drug sulfasalazine (SASP) as an xCT inhibitor (Gout et al., 2001). SASP, glutamate, monosodium glutamate, and chemical inhibitors of xCT reduce GSH, increase ROS, potentiate chemotherapeutic effects, and attenuate growth in a handful of tumor-derived cell lines in vitro and xenografts (reviewed in Lo et al., 2008a). SASP is labile and insoluble under physiological conditions, limiting anti-xCT use to preclinical experiments. Other effects ascribed to SASP include the on-target anti-inflammatory activity of an SASP metabolite, NFkB inhibition, and direct interaction with GSH in cell-free extracts.

Molecular explanations for glutamine reliance remain elusive, although the phenomenon is well described (Coles and Johnstone, 1962; Kovacević and Morris, 1972; Reitzer et al., 1979; DeBerardinis et al., 2007; Yuneva et al., 2007; Wise et al., 2008). Glutamine provides carbon and nitrogen for independent metabolic events, either directly, (e.g., nucleotide and protein synthesis), via the de-amidated product glutamate (e.g., polysaccharide synthesis, membrane antiporter activities), or via further glutamate deamination to 2-ketoglutarate (2-kg; e.g., respiratory/tricarboxylic acid (TCA) cycle substrates; reviewed in DeBerardinis and Cheng 2010). Abundant serum levels maintained by skeletal muscle reserves allow most cells to be glutamine consumers, although they may also be capable of synthesis (reviewed in Curthoys and Watford, 1995; Kovacevic and McGivan 1983). Glutaminase (GLS; *GLS*) and glutamine synthase (GS; *GLUL*) modulate intracellular glutamine/glutamate levels; GLS deamidates glutamine, producing glutamate and ammonia, while GS synthesizes glutamine from these products. Reciprocal expression precludes futile substrate cycling (Curthoys and Watford, 1995; Kovacevic and McGivan 1983). *GLS* expression levels were correlated with proliferation rate, respiratory glutamine use, and environmental glutamine reliance (Knox et al., 1970; Linder-Horowitz et al., 1969; reviewed in Wise et al., 2008). Thus *GLS* is a commonly proposed biomarker of glutamine-dependence and therapeutic target (Lobo et al., 2000; Lora et al., 2004; Wang et al., 2010, Yuneva et al., 2007; van den Heuvel et al., 2012), and *GLUL* a marker of glutamine independence (Collins et al., 1998; Kung et al., 2011).

Resurgence of interest in nutrient reliance followed realizations that oncogenes can direct nutrient uptake and dependence (reviewed in Wise and Thompson, 2010). However, as in other preclinical discoveries, findings in exemplar cell lines do not identify appropriate patient populations or estimate their sizes. For example, the metabolic effects of oncogenic Myc vary substantially between tissue types (Yuneva et al., 2012), making a simple cause-effect relationship between oncogenic Myc and glutamine dependence unlikely. Nor does restricting expectations to tumors of one tissue type improve the probable efficacy; in singular glioma lines, oncogenic Myc confers glutamine reliance (Wise et al., 2008), but studies of multiple glioma lines report little glutamine dependence (Dranoff et al., 1985). Also, naturally arising tumors without a dominant oncogenic driver may overcome nutrient scarcity by switching nutrient sources (Zielke et al., 1978), attenuating cell cycle progression (Jones et al., 2005), or other activities reported in nontransformed cells. Finally, nutritional requirements of tumors versus proliferating normal cells, rather than quiescent tissues have seldom been reported (exceptions: Iglehart et al., 1977; Jelluma et al., 2006), but are a critical part of the therapeutic development puzzle. Here we present analyses

Figure 1. Nutrient Consumption in Breast-Derived Cell Lines

(A) Comparison of two nomenclatures used to describe samples in our study. Sample numbers of each type are indicated.

(B) Fluorescence increase of cell lines after 4 hr culture with 2-NBDG or 6-NBDG-labeled glucose relative to unlabeled cultures.

(C) Population doubling times, calculated from standard growth curves.

(D) Glucose uptake at 4 hr (from B) versus glutamine consumption, derived from media depletion at 24 hr culture, normalized to cell number.

(E) Amino acid consumption by four claudin low samples that consume little glucose or glutamine compared to HMECd samples. Values derived as in (D); standard three-letter amino acid codes in key.

(F) Glutamine consumption at 24 hr versus *hGAC* GeneChip hybridization signal. Green squares on *y* axis are the average *hGAC* signals from three $CD10^+$ and three $BerEP4^+$ purified normal breast samples.

(G) Differential *hGAC* expression by basal versus luminal or ER^+ versus ER^- samples in eight clinical breast tumor data sets, downloaded from NCBI GEO and Chin et al. (2006). The t test p values are below the paired box plots. Error bars encompass highest and lowest values.

Icon codes are defined in the figure keys. Dotted lines bracket proliferating, nontumorigenic sample values. Icons represent mean values. Error bars represent one standard deviation.

See also Figure S1 and Tables S1–S3.

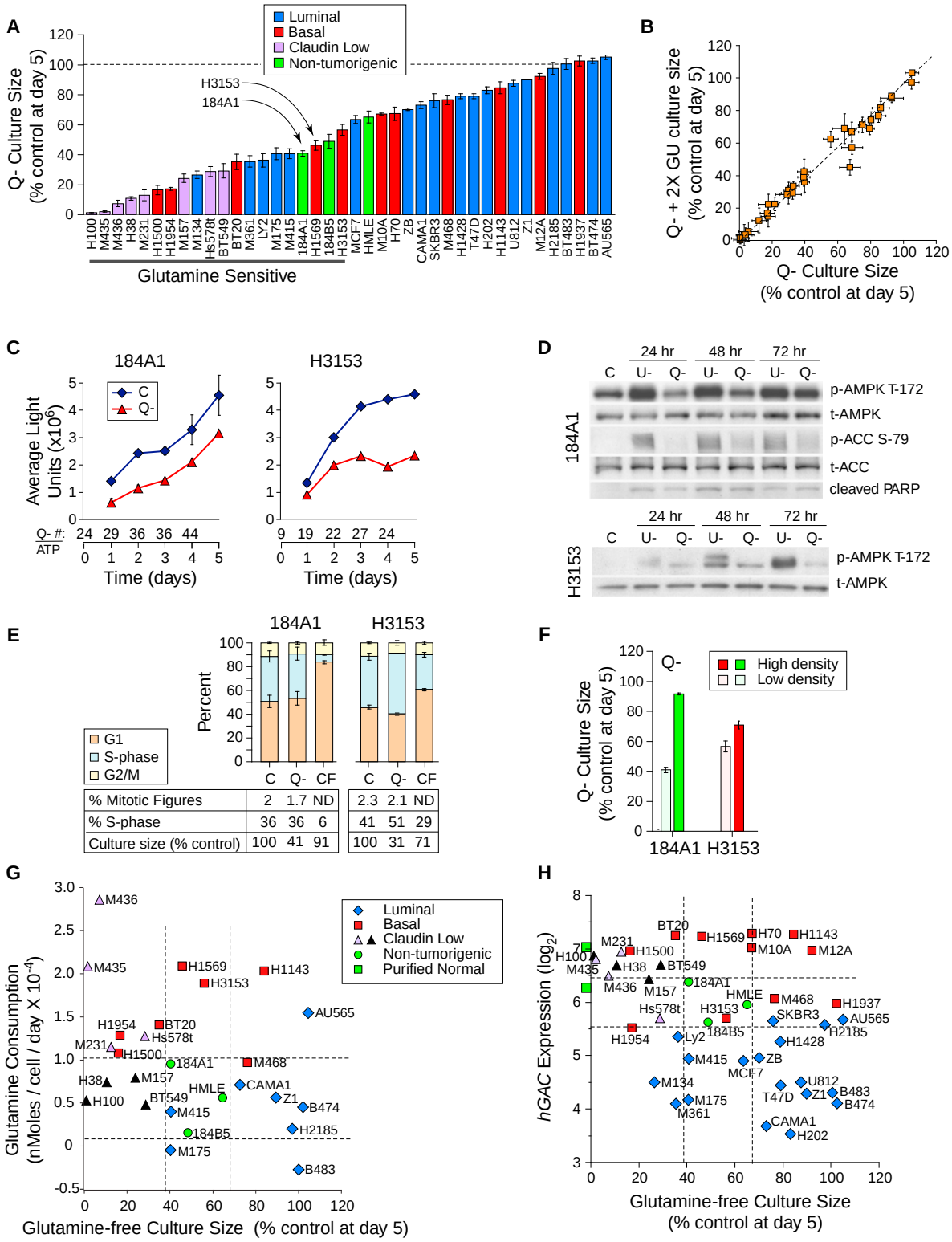

Figure 2. Glutamine Restriction Slows Culture Expansion

(A) Day 5 culture sizes for each cell line grown in glutamine-free media, normalized to culture in control media.

(B) Day 5 culture sizes in glutamine-free media with twice the normal glucose concentration (2× GU, y axis) versus glutamine-free media with normal glucose levels (x axis), each normalized to culture in control media.

(C–F) Glutamine deprivation responses in the nontumorigenic exemplar 184A1 and a similarly sensitive tumorigenic line H3153 (arrows in A) are shown. Growth curves derived from Cell Titer Glow/ATP content analysis (C). Q- #/ATP numbers are the ratio of cell numbers derived from manual counting (trypan

(legend continued on next page)

of metabolic activities implied by microarray data and identification of therapeutic targets enriched in basal and claudin low TNBC.

RESULTS

Expression profiles of culture-adapted, proliferating nontumorigenic cells (human mammary epithelial cell derivatives; HMECd); freshly purified normal breast epithelia; and purified tumor cells from patient pleural effusions were derived and merged with previously published expression profiles of 45 independently derived breast carcinoma cell lines (see Supplemental Experimental Procedures available online; Neve et al., 2006). These represent all major breast cancer subtypes and common breast oncogenes in their natural genetic contexts (Figure 1A; Table S1). Significance analysis contrasting purified tumors and tumor-derived cell lines against purified normal breast epithelia and HMECd lines identified about 760 differentially expressed probeset IDs (>30%) encoding metabolic proteins (Figure S1A; Table S2).

Nutrient Preference Varies Widely among Breast Tumors

Elevated glucose consumption relative to adjacent quiescent tissue is a canonical hallmark of tumors, but whether this is due to proliferative glycolytic demands or specific oncogenic activities is unclear. In analysis of in vitro glucose uptake rates by tumorigenic versus HMECd lines, we found highest glucose consumption in luminal carcinoma-derived isolates (Figure 1B). Claudin low TNBC and approximately one-third of basal samples consume as little or less glucose than HMECd, although they preserve many aspects of the aggressive tumors from which they are derived; (e.g., similar molecular signatures (Neve et al., 2006), rapid doubling times, (Figure 1C), and extracellular matrix invasiveness (Sommers et al., 1994, Han et al., 2010). Thus, glucose consumption varies widely among breast isolates, and tumorigenic lines do not necessarily consume more glucose than nontumorigenic proliferating cells.

Glutamine is an alternate bioenergetic substrate for many metabolic processes. In amino acid depletion analyses, we found that most basal and claudin low TNBC consume more glutamine than the luminal or HMECd samples (Figure 1D). However, at least four claudin low TNBC consume little glutamine (black triangles) and do not significantly increase consumption of another amino acid over that of the HMECd lines, with the possible exception of cystine (Figure 1E). Thus while nutrient preference often associates with molecular phenotype, the four claudin low exceptions reveal this as a generalization. Significantly enhanced nutrient consumption may not be an absolute requisite of aggressive breast tumors.

Reduced *hGAC* Expression Identifies Luminal Breast Carcinomas

We tested historical associations between glutamine consumption and glutaminase expression in our cells. Probeset IDs targeting most portions of *GLS* ($p = 0.6$, 0.9, and 0.4), and total GLS protein levels (Figure S1B, $p = 0.19$) are not statistically different between tumor molecular subtypes. However, a *GLS* carboxy terminal splice variant (*hGAC*) is reduced in luminal carcinomas (Figure 1F; *hGAC*: 221510_s_at; $p = 3.1 \times 10^{-9}$; Elgadi et al., 1999; Figure S1C). *hGAC*, but not other *GLS* probeset ID signals, are also lower in ER^+ and luminal tumors compared to ER^- and basal tumors in eight of eight clinical breast tumor microarrays examined (Figure 1G; Table S3). Thus reduced *hGAC* expression is a strong indicator of luminal carcinoma identity (t test luminal versus all $p = 4.1 \times 10^{-13}$). While *hGAC* expression and glutamine consumption modestly correlate (Figure 1F, $p = 0.005$), the exceptions in our panel (black icons between dotted vertical lines) reveal that *hGAC* and *GLS* probeset IDs poorly identify high glutamine consumers.

Glutamine Restriction Slows Expansion of Most Breast Cell Lines

Comparison of glutamine restriction responses between tumorigenic and HMECd samples revealed that 68% of luminal and 54% of basal TNBC samples were more restriction-resistant than HMECd (Figure 2A). Restriction deficits were not rescued by increasing the glucose concentration 2- or 5-fold (Figure 2B, 2× glucose; 5× not shown), suggesting that cells do not simply switch nutrients like fibroblasts and Erlich ascites (Zielke et al., 1978; Kvamme and Svenneby, 1961) to exhaust media glucose. Growth curves of HMECd and similarly sensitive tumor lines revealed that glutamine restriction simply slows culture expansion of each cell type (Figure 2A, examples at arrows; Figure 2C; Figure S2A). Unlike glucose restriction, glutamine restriction produces little AMPK activation (T-172 phosphorylation) indicative of ATP depletion, and little ACC phosphorylation that would inhibit fatty acid synthesis (Figure 2D). Only a modest increase in cell number/ATP ratios (Figure 2C, Q^- #/ATP) and little evidence of apoptosis by Annexin V staining (data not shown), PARP cleavage (Figure 2D), or nuclear morphology (Figures S2B–S2E) are seen. Day 5 cell cycle fractions and mitotic figure counts are also unchanged (Figure 2E). Culture confluence reduces S-phase fractions and glutamine sensitivity, indicating that proliferative drive imparts glutamine reliance (Figure 2E C versus CF, percent S-phase; Figure 2F). These data predict that normal proliferating breast progenitors and most breast tumors would survive a glutamine-restricting therapeutic by simply slowing expansion rates. Glutamine-free culture sizes do not correlate

blue)/ATP values. Comparison of AMPK activating phosphorylation, PARP cleavage, and ACC inhibitory phosphorylation is shown (D). Cell cycle distribution, mitotic figure counts, S-phase fractions, and culture sizes at day 5 culture in indicated conditions (E). CF, confluent cells in complete media. Day 5 culture sizes differences for high-density versus low-density cultures in glutamine-free media (F).

(G) Glutamine consumption (from Figure 1D) versus glutamine-free culture sizes from (A).

(H) *hGAC* GeneChip hybridization signal versus glutamine-free culture sizes from(A). Green squares on the y axis are the average *hGAC* hybridization signals from three $CD10^+$ and three $BerEP4^+$ purified normal breast samples.

Dotted lines bracket nontumorigenic sample values; C, complete media; Q^-, glutamine-free media; and U^-, glucose-free media. Icon codes are defined in the figure keys. Icons represent mean values. Error bars represent one standard deviation. See also Figure S2.

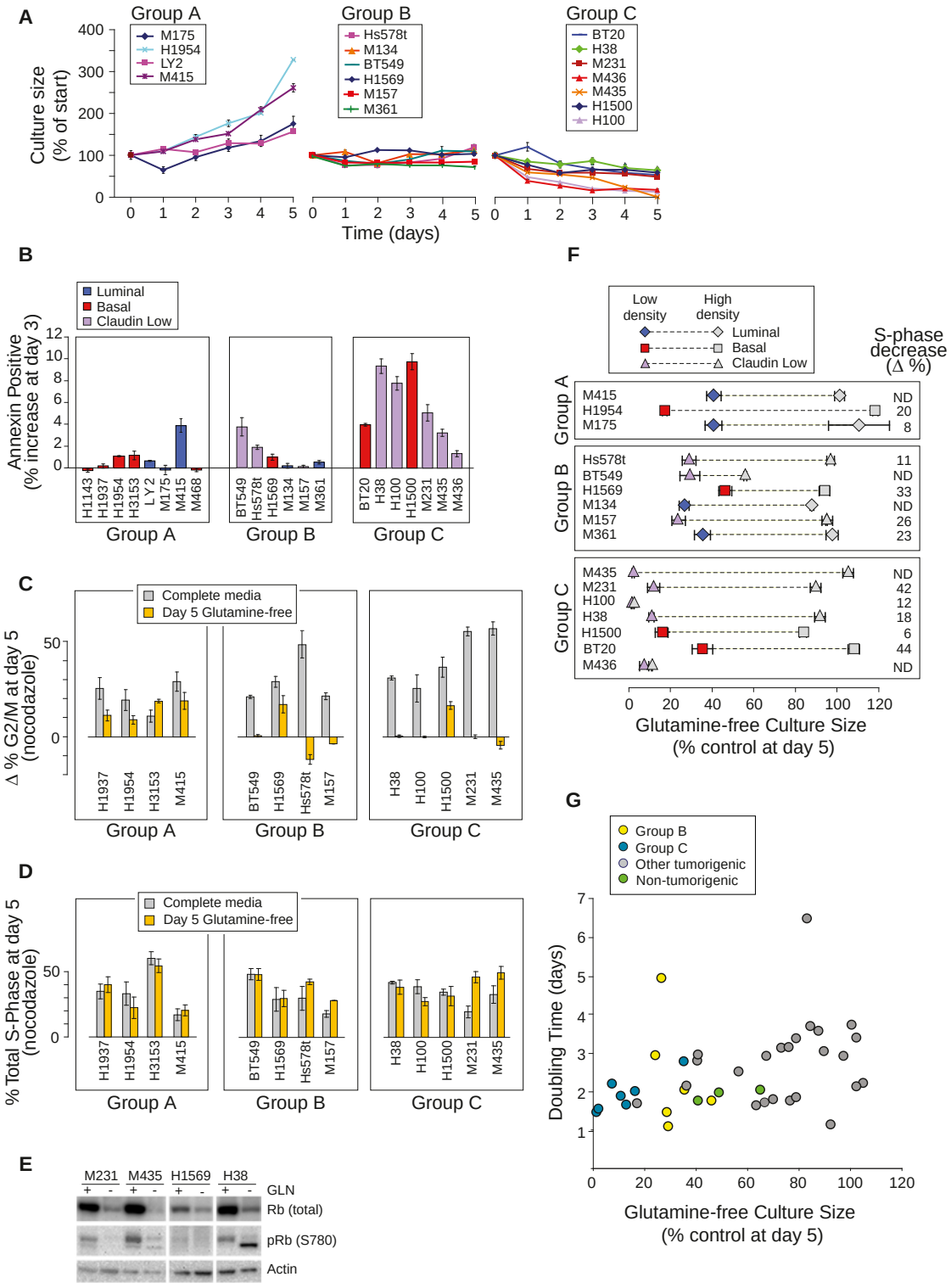

Figure 3. Glutamine Restriction Induces S-Phase Stalling in a Subset of Basal TNBC

(A) Growth curves of "glutamine-sensitive" carcinomas (underlined in Figure 2A) in glutamine-free media.

(B) Percent increases in annexin V reactivity of cells in glutamine-free media at day 3. Group averages: A, 0.8%, ± 1.4; B, 1.2% ± 1.4; and C, 5.8% ± 3.2; t test A versus C $p = 0.005$.

(C) Paired bars representing the change in percent of cells in G2/M (Δ% G2/M) with nocodazole treatment at day 5 in control (gray) versus glutamine-free (yellow) media, using cell-cycle-curve-fitting software (FLOJO, Treestar).

(D) Paired bars representing the percent S-phase fraction with nocodazole treatment of day 5 cultures in control (gray) versus glutamine-free (yellow) media.

(legend continued on next page)

with glutamine consumption (Figure 2G, p = 0.13) or *hGAC* expression (Figure 2H, p = 0.014). We conclude that historical correlations between these parameters are not applicable to breast tumors.

Restriction Induces S-Phase Stalling in a Subset of TNBC

Growth curves of the most restriction-sensitive tumors (Figure 2A, "glutamine sensitive" underbar) revealed cultures that (1) continued expansion, similar to HMECd; (2) did not significantly expand; and (3) decreased (Figure 3A). Groups B and C (B+C) include two ER^+ (luminal) and 11 TNBC (three basal, eight claudin low) independently derived samples, including the four claudin low cells that consume little glutamine (Figures 1D, black). Group C cells increase Annexin V reactivity (Figure 3B) and apoptotic figures (Figure S3A) on days 2–4 of restriction. Thus approximately one-half of our TNBC lines are unable to survive or expand without glutamine.

We tested whether the few live cells in day 5 group B+C cultures had arrested in G1, reasoning that they might survive glutamine restriction to seed tumor recurrences, discouraging development of glutamine-restricting therapeutics. In complete media, nocodazole treatment increased G2/M and late S-phase fractions of all samples tested, demonstrating transit to and activation of an intact mitotic checkpoint (Figure 3C, gray bars; late S-phase data not shown; Figure S3B). Glutamine-free cultures of group A exemplars exhibited similar G2/M increases (gray versus yellow bars), but not group B or C samples. The unchanged S-phase fractions rule out G1 arrest by group B+C samples (Figure 3D, paired gray versus yellow bars). Their cell cycle profiles are identical with or without nocodazole treatment (Figure S3C), indicating S-phase stalling, with reduced total and phosphorylated retinoblastoma proteins similar to S-phase stalling in DNA damage responses (Figure 3E, Knudsen et al., 2000). However, like glutamine-restricted Myc-transformed fibroblasts, γH2A.X phosphorylation is not increased, indicating that the intra-S-phase DNA damage checkpoint remains inactive (data not shown; Yuneva et al., 2007). Culture confluence reduces the S-phase content and glutamine sensitivity of all but two group C samples (Figure 3F, colored versus gray icons). However, group B+C samples are not simply the most rapidly dividing cells (Figure 3G; t tests: all versus C+B, p = 0.11; all basal and claudin low versus C+B, p = 0.2), indicating that they harbor specific defects that make them unable to surmount restriction.

Known Regulators of Glutamine Metabolism Do Not Identify Group B or C Cells

We tested proposals that *hGAC* and *GLUL* identified glutamine-dependent cells. While *hGAC* statistically identifies group C ($p = 5.6 \times 10^{-9}$) and group B+C (p = 0.008) cells, only 9/13 (69%) samples expressing higher *hGAC* than HMECd cells are group B or C (Figure 4A, above upper dotted line), and these levels are similar to purified normal epithelia (green squares). *hGAC* also poorly discerns group C (p = 0.03) or B+C (p = 0.17) from all other TNBC. While *GLUL* levels correlate with restricted culture sizes (Figure 4B; p = 0.005–$2.3 \times^{-4}$, three probeset IDs; Figure S4A), *GLUL* also more accurately discerns luminal from claudin low samples (Figure 4B; $p = 1.9 \times 10^{-5}$). At lower p values, *GLUL* discerns luminal from all basal + claudin low ($p = 2.5 \times 10^{-5}$ to 1.9×10^{-4}), or ER^+ from ER^- ($p = 4.4 \times 10^{-3}$ to 1.2×10^{-2}) cell lines, and samples in seven of eight clinical expression data sets (Figure 4C; Table S4). Most group B+C cells express less *GLUL* than normal samples (Figure 4D), but low expression is not unique to group B+C (gray circles below lower dotted line). Nor can *GLUL* discern group C (p = 0.20–0.67) or B+C samples (p = 0.015–0.09) from other TNBC. Thus, *hGAC* and *GLUL* are not strong biomarkers for group B or C type tumors.

Oncogenic Myc can drive glutamine uptake and dependence in exemplar fibroblasts and glioma (Wise et al., 2008; Gao et al., 2009; Yuneva et al., 2007). *CMYC* is enriched in our basal and claudin low cells (p = 0.013). But neither *CMYC*, other Myc family members, or core MYC expression signature genes (Chandriani et al., 2009) are differentially expressed in group C or group B+C cells versus other basal + claudin low cells (Figure S4B; Table S5). We also found no correlation between *TP53* mutational status and group B or C membership using the IARC TP53 database (see Supplemental Experimental Procedures, p = 0.7; http://p53.iarc.fr/CellLines.aspx). Significance analysis contrasting gene expression in the group C or B+C samples versus other basal and claudin low TNBC did not identify potential biomarkers or offer molecular explanations for S-phase stalling (data not shown).

Group B and C Carcinomas Are Glutamine Auxotrophs

Glutamine restriction reduces *hGAC* and *GLUL* mRNA levels in low-density cultures, while producing little change in GS protein levels (Figures 4E, 4F, S4C, and S4D). Confluent cultures can induce *GLUL* mRNA (Figure 4E, e.g., M435), suggesting one mechanism for their starvation resistance. But we conclude that proliferating breast tumors cannot induce *GLUL* to escape glutamine restriction.

Titrations of 17 common carbon sources over four concentration logs were tested for rescue of an exemplar group C carcinoma (M436) from glutamine restriction (Figure S4E). Neither these nor nitrogen sources, ammonium chloride, choline chloride, or putrescine, improved cultures (Figure S4F). Only glutamate (2- to 3-fold), oxaloacetate (2%–6%), and dimethyl 2-ketoglutarate (2%–10%; Figure S4G) increased ATP values slightly; however, only glutamate increased viable cell numbers in multiple group C cell lines (4%–6%; Figure S4H). Combining GS substrates, glutamate and nitrogen sources, did not further improve cultures (Figure S4I). We conclude it unlikely that other commonly available nutrients can substitute for glutamine during restriction, and that the group C+B tumors are functional glutamine auxotrophs.

(E) S-phase stalling is accompanied by a decrease in total and serine 780 phosphorylated retinoblastoma protein.
(F) Culture confluence reduces S-phase fractions and glutamine sensitivity; S-phase decrease (Δ%) is the decrease in percent S-phase with high density culture (gray icons) versus low density culture (colored icons); paired icons connected by dashed lines represent a single cell line.
(G) Doubling time (from Figure 1C) versus glutamine-free culture sizes (from Figure 2H).
Icon codes are defined in the figure keys. Icons represent mean values. Error bars represent one standard deviation.
See also Figure S3.

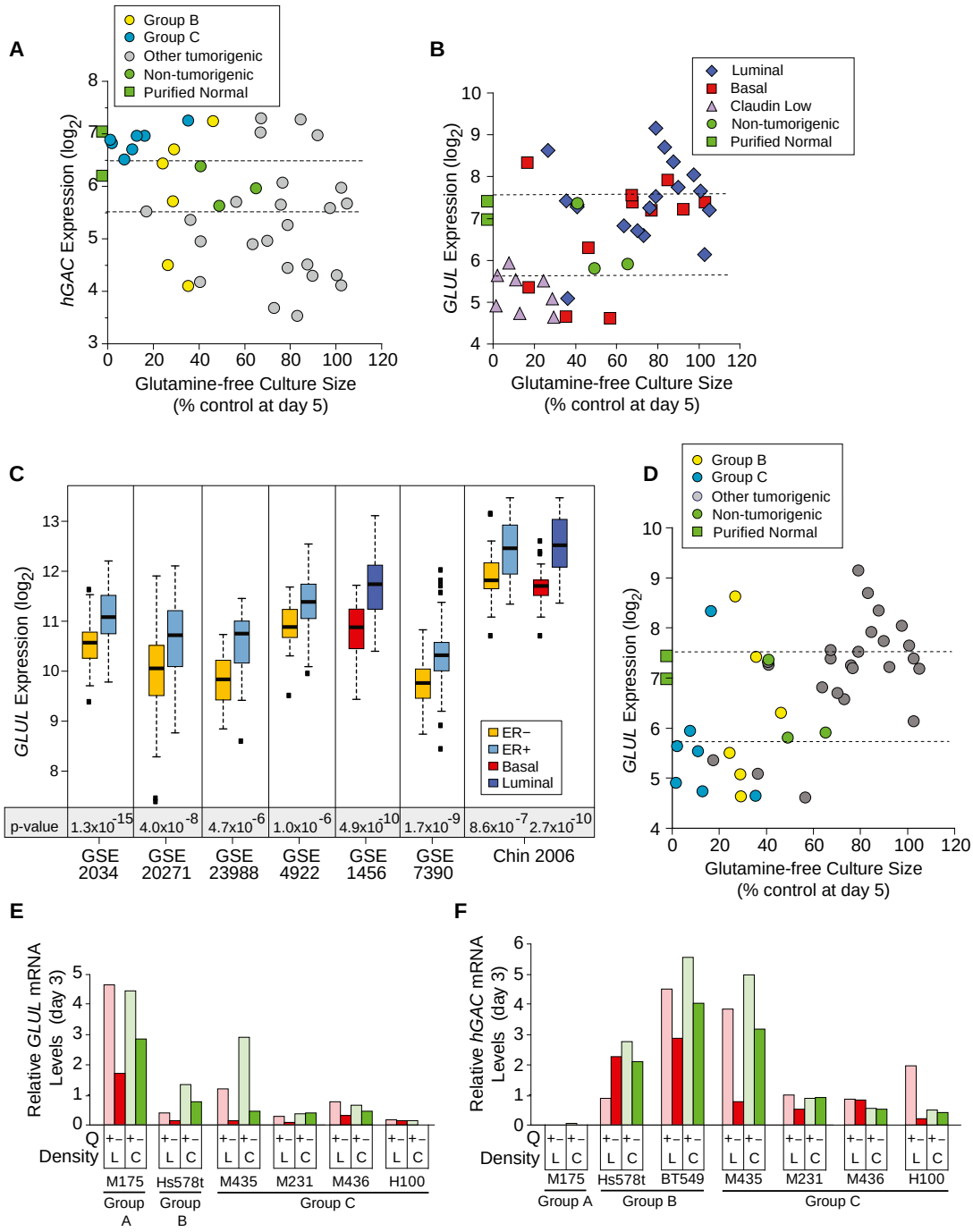

Figure 4. Common Regulators of Glutamine Metabolism Do Not Identify Auxotrophic Cells

(A) *hGAC* GeneChip hybridization signal (log_2) versus glutamine-free culture sizes (from Figure 2H) coded as restriction groups B and C versus others.

(B) *GLUL* GeneChip hybridization signal (log_2) versus day 5 glutamine-free culture sizes, coded by molecular subtype.

(C) *GLUL* expression by basal versus luminal or ER^+ versus ER^- samples in eight clinical breast tumor expression data sets, downloaded from NCBI GEO and Chin 2006 (Chin et al., 2006); t test p values are below paired boxplots. Error bars encompass highest and lowest values.

(D) Correlation of glutamine-free culture sizes and *GLUL* expression as in (B), but coded by restriction groups.

(E and F) Comparison of (E) *GLUL* and (F) *hGAC* mRNA levels at day 3 in glutamine replete versus deficient media, from quantitative PCR analysis. L, low density; C, confluent; and Q, glutamine.

Icon codes are defined in the figure keys. Green squares, average hybridization signals from three $CD10^+$ and three $BerEP4^+$ purified normal breast samples. Icons represent mean values. Error bars represent one standard deviation. Dotted lines bracket proliferating, nontumorigenic sample values.

See also Figure S4 and Tables S4 and S5.

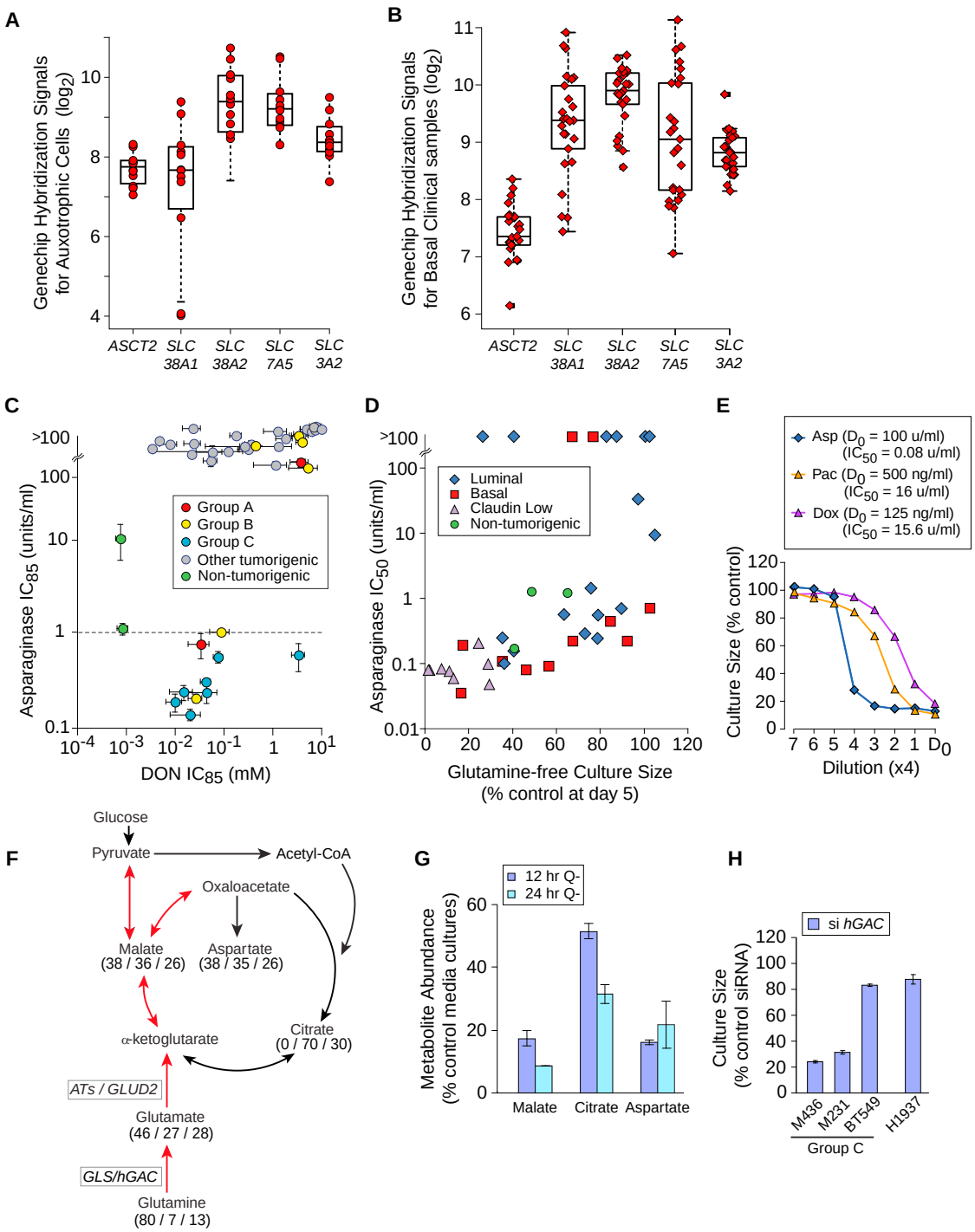

Figure 5. Glutamine Auxotrophy Presents Therapeutic Opportunities

(A) GeneChip hybridization signals for four glutamine transporters and the common heavy chain (*SLC3A2*) in glutamine auxotrophic cells. Error bars encompass highest and lowest values.

(B) GeneChip hybridization signals for transporters as in (A), for basal carcinoma subsets of clinical data sets downloaded from NCBI GEO and Chin 2006 (Chin et al., 2006), one example data set shown. Error bars encompass highest and lowest values.

(C) Relative asparaginase (y axis), and DON (x axis) sensitivities (IC_{85}) of our cell panel, coded by restriction groups B and C versus others. Dotted line, asparaginase concentration used to kill sensitive leukemia cells in vitro (1 u/ml).

(D) Day 5 glutamine-free culture sizes (from Figure 2A) versus asparaginase sensitivity (IC_{50} shown).

(E) Four-fold drug titrations and calculated IC_{50}s for an exemplar group C auxotroph (M436). D_0, highest drug concentration and calculated IC_{50}s in figure key; Asp, asparaginase; Pac, paclitaxel; and Dox, doxorubicin.

(legend continued on next page)

Glutamine Auxotrophy Presents Therapeutic Opportunities

We tested three approaches to therapeutic development targeting auxotrophic TNBC: preventing glutamine access, inhibiting glutamine-dependent enzymes, and inhibiting activities requiring glutamine metabolites. Auxotrophs (Figure 5A) and basal carcinoma subsets in clinical microarray data sets (Figure 5B, example; Table S6) express multiple glutamine transporters. Thus we prevented glutamine access by treating cultures with the leukemia therapeutic asparaginase, reducing asparagine and glutamine to their acidic derivatives (Figure S5A; Narta et al., 2007). This produced an apparent synthetic lethality at concentrations equal to that of leukemia in all group C and in approximately one-third of group B cells (Figure 5C, 85% inhibitory concentration [IC_{85}] below dotted line; Asselin et al., 1989). Correlated asparaginase sensitivities and glutamine-free culture sizes (Figure 5D, $p = 5.7 \times 10^{-6}$; asparaginase IC_{84}; $p = 9.3 \times 10^{-9}$, not shown) reveal that glutamine re-synthesis from the asparaginase products glutamate and ammonia is uncommon. We propose that local asparaginase/glutaminase delivery would kill auxotrophic tumors without requiring selective identification and targeting of their potentially varied molecular defects. Cells relatively resistant to paclitaxel or doxorubicin are exquisitely asparaginase-sensitive, indicating that an asparaginase-like therapeutic could become a critical, independent alternative for drug-resistant tumors (Figure 5E).

Analysis of ^{13}C-5-glutamine-derived metabolites in the group C TNBC M436 (Figure 5F; Table S7) revealed that 80% of intracellular glutamine is imported (all five carbon positions are ^{13}C-labeled). Approximately 40% of TCA cycle metabolites and their derivatives are directly produced from this pool, and another one-third (27%–30%) are partially ^{13}C-labeled. Glutamine restriction depletes these pools (Figure 5G), suggesting that inhibition of glutaminase (GLS/hGAC) or aminotrasferases (ATs) might kill or slow growth of the auxotrophs. siRNA-mediated reduction of *hGAC*-attenuated culture expansion of auxotrophs with high glutamine consumption rates (Figure 5H, M436, M231; Figure S5B), but provided little efficacy against BT549, an auxotroph that consumes little glutamine (Figure 1D), or H1937, a group A TNBC. In comprehensive tests, treatment with a broad spectrum inhibitor of amidotransferases including GLS (6-diazo-5-oxo-L-norleucine; DON; reviewed in Souba, 1993) placed auxotrophs among the most sensitive samples (Figure 5C). We propose that inhibitors of single DON targets should be refined for use against auxotrophic TNBC.

Glutamine Is Required for ROS Control in TNBC

Finally, we tested the strategy of inhibiting an activity that requires glutamine metabolites. In the normal human fibroblast IMR-90, one-third of glutamine uptake supplies glutamate for xCT exchange activity (Bannai and Ishii, 1988). Analysis of amino acid consumption revealed highly correlated cystine depletion and glutamate secretion in 27 of our lines (Figure 6A, $p = 8.8 \times 10^{-11}$; Figure S6A), suggesting xCT activity. Glutamine restriction strongly reduced exchange (Figure 6B), modestly decreased GSH levels (Figure 6C) and increased intracellular ROS by at least 30% in 8/19 TNBC (Figure 6D, light blue). This is partially corrected by the ROS scavenger N-acetylcysteine (NAC) in 12/13 samples (light gray). NAC does not allow culture expansion (Figure S6B), thus, glutamine use for ROS control is common, but other glutamine-influenced factors are also required for auxotroph proliferation.

We directly assessed the xCT expression and function in TNBC that was implied by the glutamine restriction effects on ROS. Basal and claudin low lines overexpress the xCT exchange-specific subunit *SLC7A11* (Figure 6E, $p = 0.06–7.4 \times 10^{-4}$; Figure S6C), the glutamate-cysteine ligase regulatory subunit of glutathione synthase (arrow; *GCLM*, $p = 0.011$), and a membrane interacting protein *CD44* $p = 0.005–5.9 \times 10^{-8}$; Ishimoto et al., 2011). Cystine consumption and *SLC7A11* mRNA levels correlate (Figures 6F and S6D), and siRNA-mediated reduction of *SLC7A11* mRNA increases intracellular ROS (Figures 6G and 6H). SASP treatment reduces cystine/glutamate exchange and GSH content (Figures 6B and 6C). 2-mercaptoethanol (2me) provides cystine as mixed 2me-cysteine disulfides (Ishii et al., 1981), and normalizes GSH levels, demonstrating SASP specificity for cystine and GSH production. In 18/19 TNBC, SASP increases endogenous ROS by at least 50% (Figure 6D, teal bars), which are reduced by NAC in 14/16 samples (dark gray bars). Using reagents for specific ROS species, we found that SASP increases hydroxyl radicals, in keeping with the expected effects of GSH depletion (Figure S6E; Franco et al., 2007). Thus, the xCT antiporter is commonly expressed and functional in TNBC. HMECd expresses these genes (Figure 6E, columns "I"), but xCT is much less active (Figure 6A, green).

SASP Treatment Attenuates Tumor Growth

In proliferation assays, we found that SASP treatment dramatically reduces TNBC culture sizes with half-maximal inhibitory concentration (IC_{50}) values modestly correlated to cystine uptake in complete media (Figure 7A, $p = 0.07$). Culture sizes are significantly restored by NAC (Figure 7B) and not affected by the active anti-inflammatory fragment of SASP, 5-aminosalicylic acid (5-ASA; Figure S7A). Thus inhibition of cystine acquisition, not anti-inflammatory activity, is responsible for TNBC proliferative sensitivity. This concentration range (0.2–0.7 mM) is not far from serum concentrations measured in bowel inflammatory patients (0.18 mM; Guastavino et al., 1988). Under normoxic conditions (5% O_2), SASP sensitivity increased 2- to 3-fold (Figure S7B), and SASP significantly slowed growth of an auxotrophic line xenograft (Figure 7C), indicating that xCT activity is also critical for growth in vivo. Accordingly, 8/20 anonymous TNBC clinical specimens strongly express xCT (Figure 7D and S7C–S7K). TNBC can be treated with carboplatin, and

(F) TCA cycle diagram illustrating respiratory use of glutamine in red arrows. Numbers indicate mass spectroscopy determination of the percent of each metabolite that contains (all/several/no) ^{13}C-carbons derived from culture with ^{13}C-5-glutamine in M436.
(G) Decrease in key TCA cycle metabolite pools with glutamine restriction, expressed as percent control media cultures. Q^-, glutamine-free media.
(H) Proliferative effects of siRNA-mediated *hGAC* mRNA reduction in exemplar cell lines, expressed as a percent of transfection with a scrambled siRNA.
Icon codes are defined in the figure keys. Icons represent mean values. Error bars represent one standard deviation.
See also Figure S5 and Tables S6 and S7.

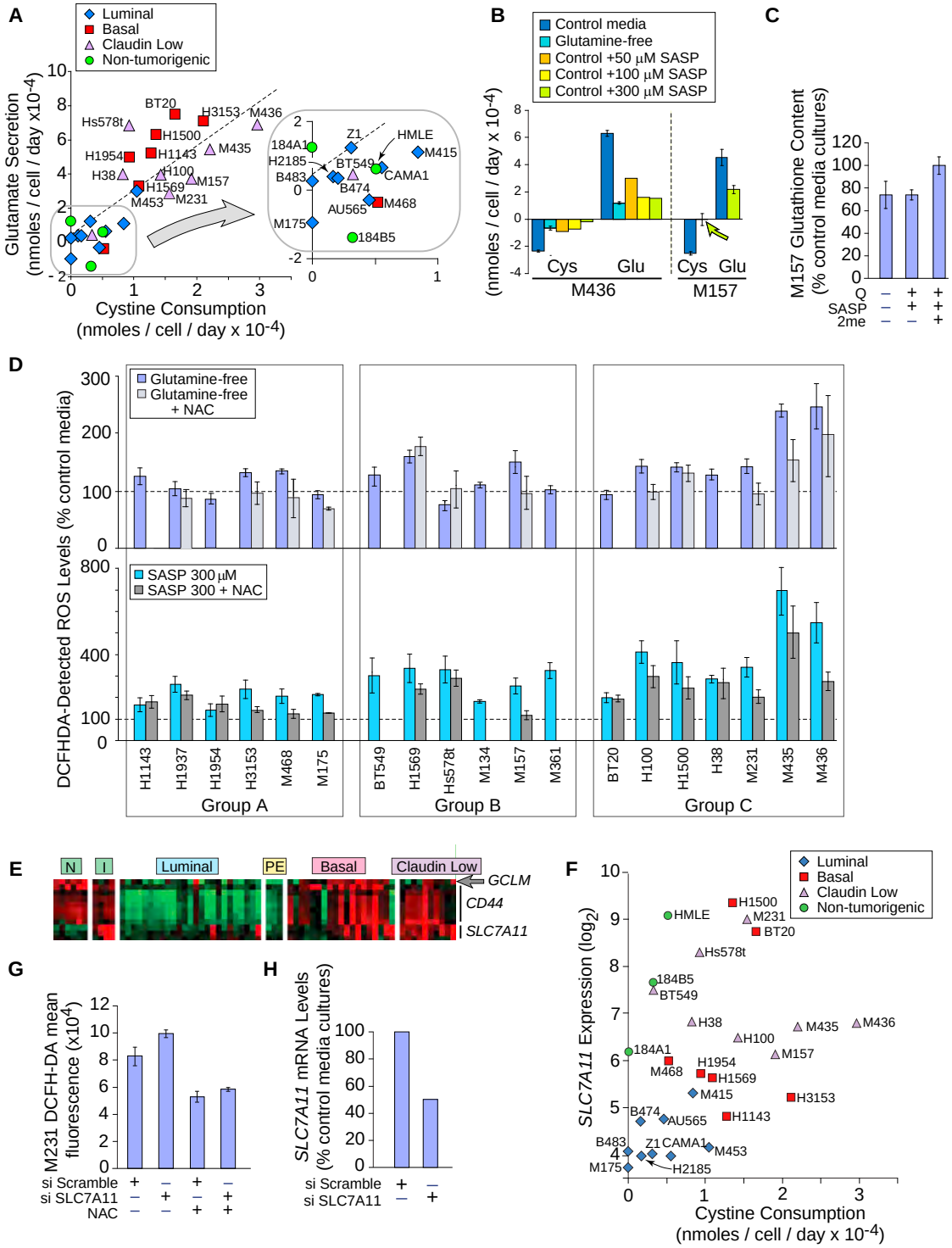

Figure 6. Glutamine Restriction and xCT Inhibition Increase ROS

(A) Change in media cystine (x axis) and glutamate (y axis) concentrations of cells cultured 24 hr in control media.

(B) Twenty-four hr of glutamine restriction or SASP treatment reduces cystine/glutamate exchange by exemplar group C auxotrophs. cys, cystine and glu, glutamate.

(C) Effects of 24-hr glutamine restriction or SASP treatment on GSH content in an exemplar group C TNBC; Q, glutamine-free media; SASP, SASP treatment in complete media; and SASP + 2me, SASP treatment in the presence of beta-mercaptoethanol.

(D) ROS levels in basal carcinomas assessed with DCFHDA fluorescence, normalized to control media reactivity. Light blue, 2-day cultures in glutamine-free media. Group averages: A, 112% ± 21; B, 121% ± 31; C, 162% ± 59; t test group A versus C, p = 0.07; and group A versus B+C, p = 0.074. Light gray,

(legend continued on next page)

carboplatin + SASP reduces the carboplatin IC_{50} in 13/14 of our TNBC samples (Figure 7E). We propose that SASP be derived for clinical use.

DISCUSSION

Rodent breast tumors (Erlich Ascites series) were instrumental in the definition of central metabolic pathways and tumor-specific aberrations, but work in human breast tumors is largely limited to aspects of fatty acid metabolism (see Menendez and Lupu, 2007). Reports of other metabolic features are less frequent and use only one or a few samples, producing biased conclusions due, for example, to the mistaken use claudin low lines to represent typical TNBC; misidentification of GeneChip probeset IDs that are *hGAC* splice variant specific as reporting total *GLS* mRNA; the lack of gene expression comparisons between tumors and normal breast epithelia; and the inability to directly compare nontumorigenic breast derivative and tumorigenic behaviors (for examples, see Collins et al., 1998; Kung et al., 2011; Simpson et al., 2012). Our data clarify these misunderstandings and provide a detailed nutrient utilization portrait of a comprehensive organ site-specific tumor collection, contrasting gene expression and functional assays to define common nutrient utilization patterns and responses to drugs that leverage associated metabolic activities.

Historically Associated Metabolic Features Vary Substantially in Breast Cancer

Doubling time, glutamine consumption, and glutamine reliance are historically correlated. Among this triad, only doubling time and glutamine-free culture sizes modestly correlate across our large sample collection (Figure 3G, $p = 0.002$). However, the glutamine auxotrophs are not simply the most rapidly dividing samples. Nor are they the largest glutamine consumers; four of eight auxotrophic, claudin low samples consume no more glutamine than proliferating nontumorigenic cells (Figure 1D, black triangles: BT549, H38, H100, M157). Glutamine can be cycled by import via ASCT2 and export in exchange for essential amino acids via the LAT1/4f2hc antiporter (*SLC7A5/SLC3A2,* Figure 7F, dark blue arrows; Nicklin et al., 2009). Our four low glutamine consumers express all antiporter components (Figure 5A), and glutamate cycling would not deplete measured ambient glutamine levels. Thus, these cells may require glutamine to fuel both this exchange activity and the xCT antiporter and use relatively less glutamine for respiration. This may explain the relative proliferative resistance to siRNA-mediated reduction of *hGAC* seen in BT549 (Figure 5H). Differences between glutamine cycling and catabolism may also partially explain historically variable correlations between glutamine uptake and glutamine reliance in other tumors.

Conversely, auxotrophs of high glutamine consumption (Figure 1D; M436) that require glutamine as a major respiratory fuel (Figures 5F and 5G; Figure 7F, light blue arrows) and for glutamate/cystine exchange (Figures 6B and 7F, gray arrows), may be more susceptible to inhibition of *hGAC* (Figure 5H; M436, M231) and subordinate glutamate-dependent activities such as aminotransferases (ATs; Thornburg et al., 2008). Thus within a single tumor cell line, multiple critical requirements for glutamine may exist and provide multiple therapeutic targets, either individually or in combination. We hypothesize that xCT inhibition may be further potentiated by limiting glutamate availability (Figure 7F).

Historically Proposed Genetic Indicators of Glutamine Reliance Do Not Define Auxotrophy

With the resurgent interest in tumor metabolism, metabolic genes such as *GLS* and *GLUL* have been re-asserted as potential therapeutic targets and biomarkers, but we find that therapeutic relevance is not so easily defined. Gene expression may suggest metabolic behaviors that are more likely active in specific tumor groups, such as a statistical association of *hGAC* with high glutamine consumption in basal and claudin low versus luminal tumors (Figures 1F). However, neither *hGAC* nor *GLUL* defines high glutamine consumption or identifies the true auxotrophic group B and/or C cells with appropriate sensitivity to be considered independent clinical biomarkers. We also find that responses to interruption of ongoing metabolic activities can vary substantially due to unknown cell-intrinsic factors. For example, individual tumors can respond to glutamine restriction by slowing culture expansion or stalling in S-phase and dying (Figures 3A–3C). Molecular explanation(s) for S-phase stalling remain unclear and may be due to tumor defects far removed from direct glutamine interaction.

xCT Is a Compelling Therapeutic Target for Triple-Negative Tumors

Inhibitor and RNAi studies reveal xCT induction as the dominant means of increasing cystine acquisition to accelerate GSH synthesis (reviewed in Lo et al., 2008a). Thus xCT may be a target for cell-specific GSH depletion, because SASP and other xCT inhibitors can slow growth of exemplar cell lines in xenograft without significant effects on other organs and can cooperate with chemotherapeutics such as cisplatin (Okuno et al., 2003), geldanamycin (Huang et al., 2005), doxorubicin (Narang et al., 2007), and gemcitabine (Lo et al., 2008b). Currently, the SASP structure is labile, designed to be cleaved by enteric bacteria to release an active anti-inflammatory fragment. It is also insoluble in aqueous solutions and not optimized for the fortuitous interaction with xCT. Thus while direct clinical applications to TNBC are unrealistic, SASP is a strong lead compound for development of xCT

glutamine-free media +NAC. Teal, cultures treated 24 hr with SASP. Group averages; A, 205% ± 43; B, 287% ± 62; C, 405% ± 168; t test group A versus C, $p = 0.019$; and group A versus B+C, $p = 0.003$. Dark gray, SASP +NAC.

(E) Heatmap of genes involved in xCT function: red, increased and green, decreased; N, purified normal $CD10^+$ and $BerEp4^+$ breast epithelial cells; I, proliferating nontumorigenic cell lines; and PE, ER^+ tumor cells purified from pleural effusions.

(F) *SLC7A11* GeneChip hybridization signal (log_2) versus cystine consumption, icons coded by molecular subtype.

(G) ROS levels in M231, 48 hr after targeting *SLC7A11* or a scrambled siRNA, in the presence or absence of N-acetylcystine (NAC).

(H) *SLC7A11* knockdown efficiency of siRNAs used in (G).

Icon codes are defined in the figure keys. NAC, N-acetylcystine and SASP, sulfasalazine. Icons represent mean values. Error bars represent one standard deviation. Amino acid quantitation obtained with HPLC. See also Figure S6.

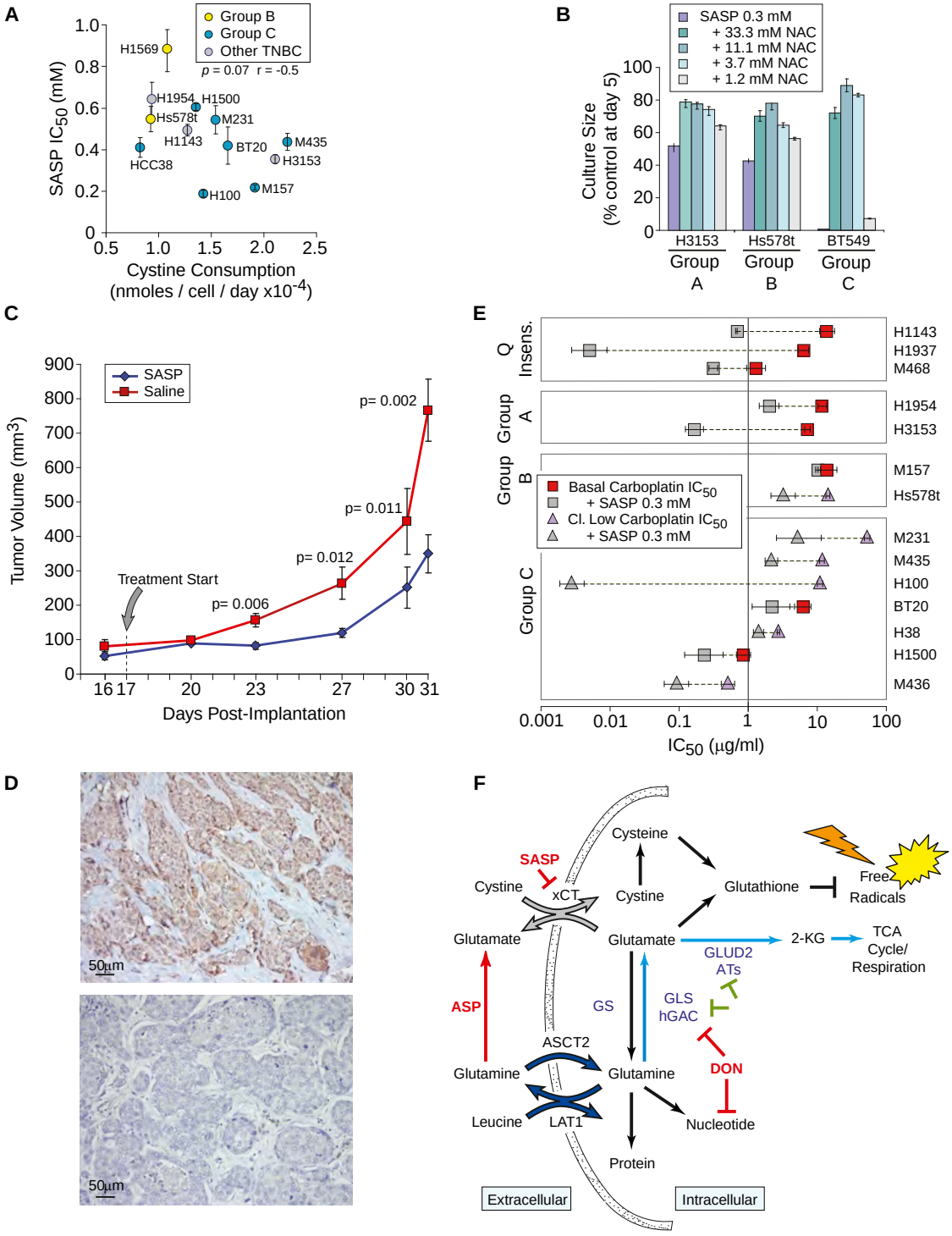

Figure 7. SASP Attenuates Proliferation In Vitro and In Vivo

(A) Cystine consumption in complete media derived from HPLC analysis (*x* axis) versus SASP sensitivity (IC_{50}).

(B) NAC treatment rescues SASP-induced culture size defects in an exemplar cell from each restriction group A–C.

(C) SASP treatment attenuates xenograft growth; group average tumor volumes separation p values noted on graph.

(D) Examples of xCT expression in exemplar human TNBC tumor sections. Nuclei, blue and xCT-specific HRP signal, brown; upper positive, lower negative.

(E) SASP reduces the carboplatin IC_{50} of most basal TNBC; paired icons connected by dashed lines represent a single TNBC. Colored icons, carboplatin IC_{50}; gray icons, IC_{50} of carboplatin plus 300 μM SASP; and Q insens., basal TNBC with less glutamine-sensitivity than non-tumorigenic cells.

(F) Summary of discussed glutamine catabolic activities. Red, compounds tested in this manuscript; green, activities with potential therapeutic inhibitory importance in glutamine-avid TNBC; dark blue, LAT1 glutamine/leucine antiporter and ASCT2, system ASC glutamine transporter; gray, xCT, the

(legend continued on next page)

inhibitory therapeutics. Our studies reveal that *SLC7A11* expression, cystine/glutamate exchange activity (Figures 6A, 6E, and 7D), and deleterious proliferative effects of xCT inhibition are common in basal and claudin low carcinomas (Figures 7A and 7C). *CD44* and the claudin low gene expression signature associate with breast cancer stem-cell phenotypes (Hennessy et al., 2009, Prat et al., 2010), implying that SASP-derived therapeutics may target breast tumor stem cells. This is reminiscent of CD44 and xCT-dependent ROS regulation in gastric tumor progenitors (Ishimoto et al., 2011). Thus we have identified a compelling therapeutic target commonly expressed by breast tumors of poorest prognosis, and a lead compound for rapid, effective drug development.

EXPERIMENTAL PROCEDURES

Data Set Preparation
See Supplemental Experimental Procedures.

Cell Culture
Tumorigenic cell lines were adapted to RPMI or DMEM + 5% FBS (GIBCO 11875 and 11965; Table S2). Culture expansion assays performed at least three times in triplicate, in 96-well format. Relative cell number was determined (Cell Titer Glow, Promega) and verified with microscopy. Averages reported ±SD (see Supplemental Experimental Procedures and below).

siRNA Effects
Transfections (Oligofectamine, Life Technologies 12252-011) used *SLC7A11* (SilencerSelect Validated s24291, Life Technologies), *hGAC* (Dharmacon custom synthesis, sense: GGAAAGUCUGGGAGAGAAAUU, antisense: UUU CUCUCCCAGACUUUCCUU), or nonspecific siRNAs (sc-37007, Santa Cruz Biotechnology; SN-1002, Bioneer), in triplicate sub-confluent six-well or 96-well plates and the Life Technology protocol. RNA and ROS quantitation were performed at day 2.

Glucose Uptake
Cultures in Dulbecco's modified Eagle's medium/low glucose (GIBCO 11885), RPMI, or HMEC (Medium 171, Cascade Biologics), were treated with or without 2-NBDG or 6-NBDG glucose (30 μM, Molecular Probes N13195, N23106) for 0–8 hr, harvested, external fluorescence quenched (0.4% trypan blue), and 30,000 cells analyzed in triplicate FACSCalibur (Becton Dickinson) or C6 Flow Cytometer (Accuri). Average mean fluorescence values at 4 hr normalized to unstained controls are reported as ± SD.

ROS Detection
Cells were incubated for 15 min with 10 μM 2′,7′-dichlorofluorescein diacetate (DCFH-DA, Sigma D6883), or 1 hr with 5 μM 3′-(p-hydroxyphenyl) fluorescein (HPF, Molecular Probes H36004), harvested, and 30,000 cells analyzed in triplicate by FACS, normalized to unstained controls. Average mean fluorescence values are reported as ± SD.

GSH Quantitation
We used the ApoGSH Glutathione Detection Kit (BioVision) per manufacturer's instructions in triplicate with 2-me at 60 μM. Average values are reported as ± SD.

Amino Acid Analysis
Supernatants from 24-hr subconfluent duplicate or triplicate cultures and cell-free media were analyzed using standard high-performance liquid chromatography (HPLC) techniques (Biochemical Genetics Laboratory, Stanford University; UC Davis Genome Center, UC Davis). Values were subtracted from media controls, normalized to cell number. Average values are reported as ± SD.

Metabolite Analysis
Cells were cultured in the presence of ^{13}C-5 labeled glutamine (Cambridge Isotope) for 0–12 hr, PBS washed, frozen (dry ice), lyophilized, pellets weighed, and homogenized in cold 60% acetonitrile (40 μl per 1 mg of protein with acetonitrile-washed glass beads). Samples were incubated for 30 min at −80°C, supernatants collected, and pellets washed (60% acetonitrile). Pooled supernatants were lyophilized, resuspended in 200 μl H_20, and 40 μl mixed with 30 μl of 40% TCA and 50 μl of 0.1 mM noreleucine (Sigma; internal standard). Lyophilized samples were silylated (50 μl acetonitrile: MTBSTFA; N-methyl-N-tert-butyl-dimethylsilyltrifluoroacetamide, Regis Chemical, Morton Grove, IL, v/v 1:1), sonicated for 3 hr, and incubated overnight. Analysis used a PolarisQ GC-ion trap mass spectrometer (ThermoFinnigan, Austin, TX) as previously described (Yuneva et al., 2012). Metabolites were identified and quantitated using XCalibur software (ThermoFinnigan). Results were normalized to dry pellet weight, and noreleucine standard. Average values are reported as ± SD.

Immunohistochemistry
Cell lines and anonymous, de-identified tumor sections (UCSF/SPORE Tissue Core, collected under UCSF Internal Review Board approval) with high and low *SLC7A11* values (Chin et al., 2006), were stained to correlate anti-xCT reactivity (Novus Biologicals NB300-318) with *SLC7A11* mRNA levels (data not shown). Detection used citrate antigen retrieval, ABC Kit (Vector Labs), and the Novus antibody-specific protocol. Commercial tissue arrays of anonymous breast tumor and normal sections with known ER/PR/Her2 status were purchased and analyzed (Biomax).

Bioinformatics
Association of *GLS* and *GLUL* expression with ER status and molecular subtype was determined in clinical microarrays available at http://www.ncbi.nlm.nih.gov/gds. Data were preprocessed (RMA algorithm in R), and analyzed with Matlab R2011a and R version 2.12.0 for MacOS X. Pearson correlations are reported; class distinctions by Student's t test.

Xenografts
The claudin low auxotroph M231 was implanted into mammary fatpad 4 in fourteen 6-week-old NSG (NOD.Cg-Prkdc^{scid} Il2rg^{tm1Wjl}/SzJ) female mice. Animals were randomized at day 16 and injected intraperitoneally twice daily with 250 μl saline or 50 mM SASP in 0.1 N NaOH pH 7.5 from days 17 to 31 (Guan et al., 2009). Tumor volume was measured twice weekly,and average values reported as ±SD. Experiments performed following UCSF Institutional Animal Care and Use Committee approval, in accordance with institutional and national guidelines.

ACCESSION NUMBERS

The NCBI Gene Expression Omnibus repository number for the Timmerman_pico dataset presented in this paper is GSE48984.

SUPPLEMENTAL INFORMATION

Supplemental Information includes Supplemental Experimental Procedures, seven figures, and seven tables and can be found with this article online at http://dx.doi.org/10.1016/j.ccr.2013.08.020.

ACKNOWLEDGMENTS

We thank the UCSF/Gladstone Genome Core for microarray dataset generation; T. Cowan, Stanford Biochemical Genetics Laboratory for HPLC amino

glutamate/cystine antiporter; light blue, glutamine anaplerosis path; SASP, sulfasalazine; ASP, asparaginase; DON, 6-diazo-5-oxo-L-norleucine; ATs, various aminotransferases; GS, glutamine synthase; GLS, glutaminase; and hGAC, carboxy-terminal splice variant of glutaminase. Not all uses of intracellular glutamine or DON targets are illustrated.
Icon codes are defined in the figure keys. Icons represent mean values. Error bars represent one standard deviation. See also Figure S7.

acid analysis; R. Higashi, CREAM, University of Louisville, for mass spectrometry; the UCSF Preclinical Therapeutics Core for xenografts; and D. Albertson, T. Tlsty, J. Korkola, and W. Kinlaw for valuable manuscript critiques. Support was provided by the National Institutes of Health, National Cancer Institute, Bay Area Breast Cancer SPORE (P50 CA 58207), grant U54 CA 112970, the Prospect Creek Foundation, the Durra Family Fund, the Mount Zion Health Fund, and a Supporting Foundation of the Jewish Community Federation.

Received: October 14, 2012
Revised: March 21, 2013
Accepted: August 23, 2013
Published: October 3, 2013

REFERENCES

Alli, E., Sharma, V.B., Sunderesakumar, P., and Ford, J.M. (2009). Defective repair of oxidative dna damage in triple-negative breast cancer confers sensitivity to inhibition of poly(ADP-ribose) polymerase. Cancer Res. *69*, 3589–3596.

Asselin, B.L., Ryan, D., Frantz, C.N., Bernal, S.D., Leavitt, P., Sallan, S.E., and Cohen, H.J. (1989). In vitro and in vivo killing of acute lymphoblastic leukemia cells by L-asparaginase. Cancer Res. *49*, 4363–4368.

Bannai, S., and Tateishi, N. (1986). Role of membrane transport in metabolism and function of glutathione in mammals. J. Membr. Biol. *89*, 1–8.

Bannai, S., and Ishii, T. (1988). A novel function of glutamine in cell culture: utilization of glutamine for the uptake of cystine in human fibroblasts. J. Cell. Physiol. *137*, 360–366.

Chandriani, S., Frengen, E., Cowling, V.H., Pendergrass, S.A., Perou, C.M., Whitfield, M.L., and Cole, M.D. (2009). A core MYC gene expression signature is prominent in basal-like breast cancer but only partially overlaps the core serum response. PLoS ONE *4*, e6693.

Chin, K., DeVries, S., Fridlyand, J., Spellman, P.T., Roydasgupta, R., Kuo, W.L., Lapuk, A., Neve, R.M., Qian, Z., Ryder, T., et al. (2006). Genomic and transcriptional aberrations linked to breast cancer pathophysiologies. Cancer Cell *10*, 529–541.

Coles, N.W., and Johnstone, R.M. (1962). Glutamine metabolism in Ehrlich ascites-carcinoma cells. Biochem. J. *83*, 284–291.

Collins, C.L., Wasa, M., Souba, W.W., and Abcouwer, S.F. (1998). Determinants of glutamine dependence and utilization by normal and tumor-derived breast cell lines. J. Cell. Physiol. *176*, 166–178.

Curthoys, N.P., and Watford, M. (1995). Regulation of glutaminase activity and glutamine metabolism. Annu. Rev. Nutr. *15*, 133–159.

DeBerardinis, R.J., and Cheng, T. (2010). Q's next: the diverse functions of glutamine in metabolism, cell biology and cancer. Oncogene *29*, 313–324.

DeBerardinis, R.J., Mancuso, A., Daikhin, E., Nissim, I., Yudkoff, M., Wehrli, S., and Thompson, C.B. (2007). Beyond aerobic glycolysis: transformed cells can engage in glutamine metabolism that exceeds the requirement for protein and nucleotide synthesis. Proc. Natl. Acad. Sci. USA *104*, 19345–19350.

DeBerardinis, R.J., Lum, J.J., Hatzivassiliou, G., and Thompson, C.B. (2008). The biology of cancer: metabolic reprogramming fuels cell growth and proliferation. Cell Metab. *7*, 11–20.

Dranoff, G., Elion, G.B., Friedman, H.S., Campbell, G.L., and Bigner, D.D. (1985). Influence of glutamine on the growth of human glioma and medulloblastoma in culture. Cancer Res. *45*, 4077–4081.

Elgadi, K.M., Meguid, R.A., Qian, M., Souba, W.W., and Abcouwer, S.F. (1999). Cloning and analysis of unique human glutaminase isoforms generated by tissue-specific alternative splicing. Physiol. Genomics *1*, 51–62.

Franco, R., Panayiotidis, M.I., and Cidlowski, J.A. (2007). Glutathione depletion is necessary for apoptosis in lymphoid cells independent of reactive oxygen species formation. J. Biol. Chem. *282*, 30452–30465.

Gao, P., Tchernyshyov, I., Chang, T.C., Lee, Y.S., Kita, K., Ochi, T., Zeller, K.I., De Marzo, A.M., Van Eyk, J.E., Mendell, J.T., and Dang, C.V. (2009). c-Myc suppression of miR-23a/b enhances mitochondrial glutaminase expression and glutamine metabolism. Nature *458*, 762–765.

Gatenby, R.A., and Gillies, R.J. (2004). Why do cancers have high aerobic glycolysis? Nat. Rev. Cancer *4*, 891–899.

Gout, P.W., Kang, Y.J., Buckley, D.J., Bruchovsky, N., and Buckley, A.R. (1997). Increased cystine uptake capability associated with malignant progression of Nb2 lymphoma cells. Leukemia *11*, 1329–1337.

Gout, P.W., Buckley, A.R., Simms, C.R., and Bruchovsky, N. (2001). Sulfasalazine, a potent suppressor of lymphoma growth by inhibition of the x(c)- cystine transporter: a new action for an old drug. Leukemia *15*, 1633–1640.

Guan, J., Lo, M., Dockery, P., Mahon, S., Karp, C.M., Buckley, A.R., Lam, S., Gout, P.W., and Wang, Y.Z. (2009). The xc- cystine/glutamate antiporter as a potential therapeutic target for small-cell lung cancer: use of sulfasalazine. Cancer Chemother. Pharmacol. *64*, 463–472.

Guastavino, E., Litwin, N.H., Heffes Nahmod, L., and Licastro, R. (1988). [Ulcerative colitis in children. Levels of salicylazosulfapyridine and sulfapyridine during treatment]. Acta Gastroenterol. Latinoam. *18*, 107–113.

Hamilton, D., and Batist, G. (2004). Glutathione analogues in cancer treatment. Curr. Oncol. Rep. *6*, 116–122.

Han, J., Chang, H., Giricz, O., Lee, G.Y., Baehner, F.L., Gray, J.W., Bissell, M.J., Kenny, P.A., and Parvin, B. (2010). Molecular predictors of 3D morphogenesis by breast cancer cell lines in 3D culture. PLoS Comput. Biol. *6*, e1000684.

Hennessy, B.T., Gonzalez-Angulo, A.M., Stemke-Hale, K., Gilcrease, M.Z., Krishnamurthy, S., Lee, J.S., Fridlyand, J., Sahin, A., Agarwal, R., Joy, C., et al. (2009). Characterization of a naturally occurring breast cancer subset enriched in epithelial-to-mesenchymal transition and stem cell characteristics. Cancer Res. *69*, 4116–4124.

Huang, Y., Dai, Z., Barbacioru, C., and Sadée, W. (2005). Cystine-glutamate transporter *SLC7A11* in cancer chemosensitivity and chemoresistance. Cancer Res. *65*, 7446–7454.

Iglehart, J.K., York, R.M., Modest, A.P., Lazarus, H., and Livingston, D.M. (1977). Cystine requirement of continuous human lymphoid cell lines of normal and leukemic origin. J. Biol. Chem. *252*, 7184–7191.

Ishii, T., Hishinuma, I., Bannai, S., and Sugita, Y. (1981). Mechanism of growth promotion of mouse lymphoma L1210 cells in vitro by feeder layer or 2-mercaptoethanol. J. Cell. Physiol. *107*, 283–293.

Ishimoto, T., Nagano, O., Yae, T., Tamada, M., Motohara, T., Oshima, H., Oshima, M., Ikeda, T., Asaba, R., Yagi, H., et al. (2011). CD44 variant regulates redox status in cancer cells by stabilizing the xCT subunit of system xc(-) and thereby promotes tumor growth. Cancer Cell *19*, 387–400.

Jelluma, N., Yang, X., Stokoe, D., Evan, G.I., Dansen, T.B., and Haas-Kogan, D.A. (2006). Glucose withdrawal induces oxidative stress followed by apoptosis in glioblastoma cells but not in normal human astrocytes. Mol. Cancer Res. *4*, 319–330.

Jones, R.G., Plas, D.R., Kubek, S., Buzzai, M., Mu, J., Xu, Y., Birnbaum, M.J., and Thompson, C.B. (2005). AMP-activated protein kinase induces a p53-dependent metabolic checkpoint. Mol. Cell *18*, 283–293.

Knox, W.E., Linder, M., and Friedell, G.H. (1970). A series of transplantable rat mammary tumors with graded differentiation, growth rate, and glutaminase content. Cancer Res. *30*, 283–287.

Knudsen, K.E., Booth, D., Naderi, S., Sever-Chroneos, Z., Fribourg, A.F., Hunton, I.C., Feramisco, J.R., Wang, J.Y., and Knudsen, E.S. (2000). RB-dependent S-phase response to DNA damage. Mol. Cell. Biol. *20*, 7751–7763.

Kovacević, Z., and Morris, H.P. (1972). The role of glutamine in the oxidative metabolism of malignant cells. Cancer Res. *32*, 326–333.

Kovacevic, Z., and McGivan, J.D. (1983). Mitochondrial metabolism of glutamine and glutamate and its physiological significance. Physiol. Rev. *63*, 547–605.

Kung, H.N., Marks, J.R., and Chi, J.T. (2011). Glutamine synthetase is a genetic determinant of cell type-specific glutamine independence in breast epithelia. PLoS Genet. *7*, e1002229.

Kvamme, E., and Svenneby, G. (1961). The effect of glucose on glutamine utilization by Ehrlich ascites tumor cells. Cancer Res. *21*, 92–98.

Linder-Horowitz, M., Knox, W.E., and Morris, H.P. (1969). Glutaminase activities and growth rates of rat hepatomas. Cancer Res. *29*, 1195–1199.

Lo, M., Wang, Y.Z., and Gout, P.W. (2008a). The x(c)$^-$ cystine/glutamate antiporter: a potential target for therapy of cancer and other diseases. J. Cell. Physiol. *215*, 593–602.

Lo, M., Ling, V., Wang, Y.Z., and Gout, P.W. (2008b). The x_c^- cystine/glutamate antiporter: a mediator of pancreatic cancer growth with a role in drug resistance. Br. J. Cancer *99*, 464–472.

Lobo, C., Ruiz-Bellido, M.A., Aledo, J.C., Márquez, J., Núñez De Castro, I., and Alonso, F.J. (2000). Inhibition of glutaminase expression by antisense mRNA decreases growth and tumourigenicity of tumour cells. Biochem. J. *348*, 257–261.

Lora, J., Alonso, F.J., Segura, J.A., Lobo, C., Márquez, J., and Matés, J.M. (2004). Antisense glutaminase inhibition decreases glutathione antioxidant capacity and increases apoptosis in Ehrlich ascitic tumour cells. Eur. J. Biochem. *271*, 4298–4306.

Menendez, J.A., and Lupu, R. (2007). Fatty acid synthase and the lipogenic phenotype in cancer pathogenesis. Nat. Rev. Cancer *7*, 763–777.

Narang, V.S., Pauletti, G.M., Gout, P.W., Buckley, D.J., and Buckley, A.R. (2007). Sulfasalazine-induced reduction of glutathione levels in breast cancer cells: enhancement of growth-inhibitory activity of Doxorubicin. Chemotherapy *53*, 210–217.

Narta, U.K., Kanwar, S.S., and Azmi, W. (2007). Pharmacological and clinical evaluation of L-asparaginase in the treatment of leukemia. Crit. Rev. Oncol. Hematol. *61*, 208–221.

Neve, R.M., Chin, K., Fridlyand, J., Yeh, J., Baehner, F.L., Fevr, T., Clark, L., Bayani, N., Coppe, J.P., Tong, F., et al. (2006). A collection of breast cancer cell lines for the study of functionally distinct cancer subtypes. Cancer Cell *10*, 515–527.

Nicklin, P., Bergman, P., Zhang, B., Triantafellow, E., Wang, H., Nyfeler, B., Yang, H., Hild, M., Kung, C., Wilson, C., et al. (2009). Bidirectional transport of amino acids regulates mTOR and autophagy. Cell *136*, 521–534.

Okuno, S., Sato, H., Kuriyama-Matsumura, K., Tamba, M., Wang, H., Sohda, S., Hamada, H., Yoshikawa, H., Kondo, T., and Bannai, S. (2003). Role of cystine transport in intracellular glutathione level and cisplatin resistance in human ovarian cancer cell lines. Br. J. Cancer *88*, 951–956.

Prat, A., Parker, J.S., Karginova, O., Fan, C., Livasy, C., Herschkowitz, J.I., He, X., and Perou, C.M. (2010). Phenotypic and molecular characterization of the claudin-low intrinsic subtype of breast cancer. Breast Cancer Res. *12*, R68.

Reitzer, L.J., Wice, B.M., and Kennell, D. (1979). Evidence that glutamine, not sugar, is the major energy source for cultured HeLa cells. J. Biol. Chem. *254*, 2669–2676.

Simpson, N.E., Tryndyak, V.P., Beland, F.A., and Pogribny, I.P. (2012). An in vitro investigation of metabolically sensitive biomarkers in breast cancer progression. Breast Cancer Res. Treat. *133*, 959–968.

Sommers, C.L., Byers, S.W., Thompson, E.W., Torri, J.A., and Gelmann, E.P. (1994). Differentiation state and invasiveness of human breast cancer cell lines. Breast Cancer Res. Treat. *31*, 325–335.

Souba, W.W. (1993). Glutamine and cancer. Ann. Surg. *218*, 715–728.

Thornburg, J.M., Nelson, K.K., Clem, B.F., Lane, A.N., Arumugam, S., Simmons, A., Eaton, J.W., Telang, S., and Chesney, J. (2008). Targeting aspartate aminotransferase in breast cancer. Breast Cancer Res. *10*, R84.

van den Heuvel, A.P., Jing, J., Wooster, R.F., and Bachman, K.E. (2012). Analysis of glutamine dependency in non-small cell lung cancer: GLS1 splice variant GAC is essential for cancer cell growth. Cancer Biol. Ther. *13*, 1185–1194.

Wang, J.B., Erickson, J.W., Fuji, R., Ramachandran, S., Gao, P., Dinavahi, R., Wilson, K.F., Ambrosio, A.L., Dias, S.M., Dang, C.V., and Cerione, R.A. (2010). Targeting mitochondrial glutaminase activity inhibits oncogenic transformation. Cancer Cell *18*, 207–219.

Weigelt, B., and Reis-Filho, J.S. (2009). Histological and molecular types of breast cancer: is there a unifying taxonomy? Nat Rev Clin Oncol *6*, 718–730.

Wise, D.R., and Thompson, C.B. (2010). Glutamine addiction: a new therapeutic target in cancer. Trends Biochem. Sci. *35*, 427–433.

Wise, D.R., DeBerardinis, R.J., Mancuso, A., Sayed, N., Zhang, X.Y., Pfeiffer, H.K., Nissim, I., Daikhin, E., Yudkoff, M., McMahon, S.B., and Thompson, C.B. (2008). Myc regulates a transcriptional program that stimulates mitochondrial glutaminolysis and leads to glutamine addiction. Proc. Natl. Acad. Sci. USA *105*, 18782–18787.

Yuneva, M., Zamboni, N., Oefner, P., Sachidanandam, R., and Lazebnik, Y. (2007). Deficiency in glutamine but not glucose induces MYC-dependent apoptosis in human cells. J. Cell Biol. *178*, 93–105.

Yuneva, M.O., Fan, T.W., Allen, T.D., Higashi, R.M., Ferraris, D.V., Tsukamoto, T., Matés, J.M., Alonso, F.J., Wang, C., Seo, Y., et al. (2012). The metabolic profile of tumors depends on both the responsible genetic lesion and tissue type. Cell Metab. *15*, 157–170.

Zielke, H.R., Ozand, P.T., Tildon, J.T., Sevdalian, D.A., and Cornblath, M. (1978). Reciprocal regulation of glucose and glutamine utilization by cultured human diploid fibroblasts. J. Cell. Physiol. *95*, 41–48.

Cancer Cell, Volume *24*

Supplemental Information

Glutamine Sensitivity Analysis Identifies the xCT Antiporter as a Common Triple-Negative Breast Tumor Therapeutic Target

Luika A. Timmerman, Thomas Holton, Mariia Yuneva, Raymond J. Louie, Mercè Padró, Anneleen Daemen, Min Hu, Denise A. Chan, Stephen P. Ethier, Laura J. van 't Veer, Kornelia Polyak, Frank McCormick, and Joe W. Gray

Inventory of Supplemental Information

SUPPLEMENTAL DATA

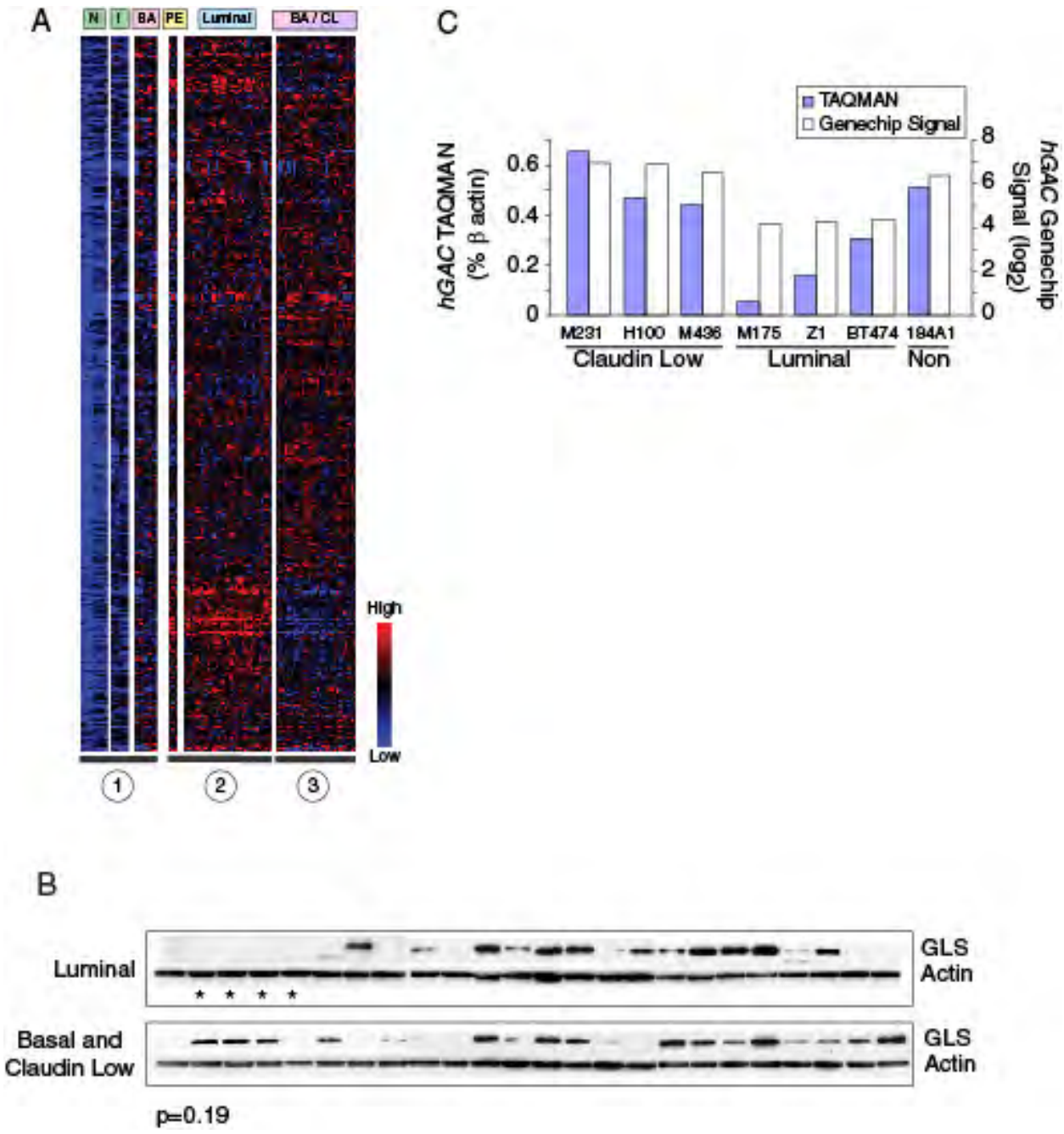

Figure S1, related to Figure 1. Molecular and Phenotypic Characteristics of Our Breast Cell Line Collection

Icon codes in figure keys. (A) Cluster and heatmap of metabolic probeset IDs identified in significance analysis comparing normal samples (1) versus Luminal (2) and Basal/Claudin low cell lines (3). Normal samples: N, purified normal $CD10^{+}$ and $BerEp4^{+}$ breast subsets; I, non-

tumorigenic culture-adapted proliferating breast cell lines derived from human mammary epithelial cells (HMECd). Tumorigenic samples: BA, Basal TNBC lines; PE, uncultured purified tumor samples from patient pleural effusions; Luminal, luminal cell lines; BA/CL, Basal and Claudin low TNBC lines. Black underbars denote major clades formed in cluster analysis. (B) Western blot assessing glutaminase expression levels in tumor-derived cell lines; pairs of sibling cell lines (asterisks) are counted as one independent isolate (AU565 and SKBR3, MCF7 and LY2); Luminal and Basal/Claudin Low cell lines do not differentially express total glutaminase protein, p= 0.19 student's t-test. (C) TAQMAN validation of relative *hGAC* Affymetrix genechip signals for representative cells in our panel.

Table S1, Related to Figure 1. Tumorigenic Cell Lines Used in This Study[1]				
Cell Line	**Abbreviated Name**	**Culture Media**	**Molecular Phenotype**	**Glutamine Restriction Group**
BT20	BT20	RPMI / 5% FBS	Basal	C
Du4475	Du4475	RPMI / 5% FBS	Basal	X
HCC1008	H1008	RPMI / 5% FBS	Basal	X
HCC1143	H1143	RPMI / 5% FBS	Basal	X
HCC1187	H1187	RPMI / 5% FBS	Basal	X
HCC1500	H1500	RPMI / 5% FBS	Basal	C
HCC1569	H1569	RPMI / 5% FBS	Basal	B
HCC1599	H1599	RPMI / 5% FBS	Basal	X
HCC1937	H1937	RPMI / 5% FBS	Basal	X
HCC1954	H1954	RPMI / 5% FBS	Basal	A
HCC2157	H2157	RPMI / 5% FBS	Basal	X
HCC3153	H3153	RPMI / 5% FBS	Basal	A
HCC70	H70	RPMI / 5% FBS	Basal	X
MDA-MB-468	M468	DMEM / 5% FBS	Basal	X
600MPE	600MPE	DMEM / 5% FBS	Luminal	X
AU565	AU565	DMEM / 5% FBS	Luminal	X
BT474	B474	RPMI / 5% FBS	Luminal	X
BT483	B483	RPMI / 5% FBS	Luminal	X
CAMA-1	CAMA1	DMEM / 5% FBS	Luminal	X
HCC1007	H1007	RPMI / 5% FBS	Luminal	X
HCC1428	H1428	RPMI / 5% FBS	Luminal	X
HCC202	H202	RPMI / 5% FBS	Luminal	X
HCC2185	H2185	RPMI / 5% FBS	Luminal	X
LY2	LY2	RPMI / 5% FBS	Luminal	A
MCF7	MCF7	RPMI / 5% FBS	Luminal	X
MCF-10A	M10A	RPMI / 5% FBS	Basal	X
MCF12A	M12A	RPMI / 5% FBS	Basal	X
MDA-MB-134VI	M134	DMEM / 5% FBS	Luminal	B
MDA-MB-175-VII	M175	DMEM / 5% FBS	Luminal	A
MDA-MB-361	M361	DMEM / 5% FBS	Luminal	B
MDA-MB-415	M415	DMEM / 5% FBS	Luminal	A
MDA-MB-453	M453	DMEM / 5% FBS	Luminal	X
SKBR3	SKBR3	DMEM / 5% FBS	Luminal	X
T47D	T47D	RPMI / 5% FBS	Luminal	X
UACC812	U812	DMEM / 5% FBS	Luminal	X
ZR-75-1	Z1	RPMI / 5% FBS	Luminal	X
ZR-75-30	Z30	RPMI / 5% FBS	Luminal	X
ZR-75-B	ZB	RPMI / 5% FBS	Luminal	X
BT549	BT549	RPMI / 5% FBS	Claudin Low	B
HBL100	H100	DMEM / 5% FBS	Claudin Low	C
HCC38	H38	RPMI / 5% FBS	Claudin Low	C
HS578t	Hs578t	RPMI / 5% FBS	Claudin Low	B
MDA-MB-157	M157	DMEM / 5% FBS	Claudin Low	B
MDA-MB-231	M231	DMEM / 5% FBS	Claudin Low	C
MDA-MB-435	M435	DMEM / 5% FBS	Claudin Low	C
MDA-MB-436	M436	DMEM / 5% FBS	Claudin Low	C

[1] Cell line name abbreviations used in this study, the normal culture media for each line, the molecular phenotype, and glutamine restriction group membership; X denotes cell lines with smaller proliferative defects in glutamine-free media than the non-tumorigenic cell lines.

Table S2, related to Figure 1. Significant Metabolic Probeset IDs.[2]			
Significant Class Association	**Probeset ID**	**Gene Symbol**	**Score**
Basal CDL	201272_at	AKR1B1	5.98627
Basal CDL	221510_s_at	GLS	5.87002
Basal CDL	202613_at	CTPS	5.75562
Basal CDL	205260_s_at	ACYP1	5.61946
Basal CDL	203909_at	SLC9A6	5.57077
Basal CDL	205996_s_at	AK2	5.44375
Basal CDL	200762_at	DPYSL2	5.26941
Basal CDL	220892_s_at	PSAT1	5.26622
Basal CDL	202026_at	SDHD	5.19516
Basal CDL	205401_at	AGPS	5.15867
Basal CDL	212174_at	AK2	5.11785
Basal CDL	205565_s_at	FXN	5.003
Basal CDL	212604_at	MRPS31	4.92187
Basal CDL	209213_at	CBR1	4.89146
Basal CDL	202589_at	TYMS	4.81951
Basal CDL	201300_s_at	PRNP	4.67459
Basal CDL	219079_at	NCB5OR	4.6724
Basal CDL	217294_s_at	ENO1	4.67206
Basal CDL	211150_s_at	DLAT	4.60905
Basal CDL	219204_s_at	SRR	4.57848
Basal CDL	219698_s_at	METTL4	4.52715
Basal CDL	218558_s_at	MRPL39	4.49672
Basal CDL	215535_s_at	AGPAT1	4.49345
Basal CDL	215707_s_at	PRNP	4.39831
Basal CDL	201012_at	ANXA1	4.37549
Basal CDL	203340_s_at	SLC25A12	4.34122
Basal CDL	221020_s_at	MFTC	4.33304
Basal CDL	205379_at	CBR3	4.33221
Basal CDL	201968_s_at	PGM1	4.30168
Basal CDL	200978_at	MDH1	4.25182
Basal CDL	221437_s_at	MRPS15	4.19826
Basal CDL	201634_s_at	CYB5-M	4.11264
Basal CDL	213133_s_at	GCSH	4.10644
Basal CDL	202502_at	ACADM	4.09831
Basal CDL	219220_x_at	MRPS22	4.0809
Basal CDL	208746_x_at	ATP5L	4.03913
Basal CDL	218982_s_at	MRPS17	3.98973
Basal CDL	202345_s_at	FABP5	3.97897
Basal CDL	214431_at	GMPS	3.96944
Basal CDL	212568_s_at	DLAT	3.95771
Basal CDL	216705_s_at	ADA	3.95428
Basal CDL	200818_at	ATP5O	3.94961
…	…	…	…

[2] Scores for metabolism-associated transcripts positively associated with the sample classes indicated in column 1, for each of three significance analyses. Analyses were: 1. Purified normal samples plus non-tumorigenic, culture adapted cells (N/I) versus carcinoma derived cell lines and uncultured pleural effusions (CDL/PE); 2. Basal carcinomas versus all other samples (Basal CDL); 3. Luminal carcinomas versus all other samples (Luminal CDL). See EXCEL file 'Timmerman Table S2 for full list.

Table S3, related to Figure 1. Class Association Statistics of *hGAC* and *GLS* Probeset IDs in Expression Datasets Derived from Primary Clinical Tumor Samples[3]

Gene Set ID	Total samp no.	Association tested	*p*-values *hGAC* 221510_s_at	*p*-values *GLS* 203157_s_at	*p*-values *GLS* 203158_s_at	*p*-values *GLS* 203159_at	*p*-values *GLS* 211414_at
GSE1561	49	- Apocrine/luminal (32) vs. basal (16) - ER status (22 ER-; 27 ER+)	3.3e-9 (basal) 0.001 (ER-)	0.514 (basal) 0.442 (ER-)	0.011 (basal) 0.015 (ER-)	0.655 (basal) 0.964 (ER-)	0.016 (basal) 0.011 (ER-)
GSE2034	286	- ER status (77 ER-; 209 ER+)	4.2e-11 (ER-)	0.060 (ER-)	3.4e-8 (ER-)	0.002 (ER-)	0.170 (ER-)
GSE20271	177	- ER status (78 ER-; 98 ER+)	1.7e-4 (ER-)	4.4e-5 (ER-)	1.6e-4 (ER-)	0.031 (ER-)	4.6e-4 (ER-)
GSE23988	61	- ER status (29 ER-; 32 ER+)	2.4e-7 (ER-)	0.089 (ER-)	0.010 (ER-)	0.278 (ER-)	0.364 (ER-)
GSE4922	289	- ER status (34 ER-; 211 ER+)	5.3e-10 (ER-)	0.969 (ER-)	0.026 (ER-)	0.527 (ER-)	0.087 (ER-)
GSE1456	159	- Luminal A/B (62) vs basal (25)	1.2e-8 (basal)	0.173 (basal)	0.002 (basal)	0.003 (basal)	0.080 (basal)
GSE7390	198	- ER status (64 ER-; 134 ER+)	1.2e-7 (ER-)	0.060 (ER-)	1.4e-6 (ER-)	0.041 (ER-)	0.003 (ER-)
Chin 2006	118	- ER status (43 ER-; 75 ER+) - Subtype Euclidean-based (66 lumA/B; 28 basal) - Subtype correlation-based (61 lumA/B; 30 basal)	4.5e-8 (ER-) 2.2e-13 (basal) 4.7e-13 (basal)	ND	ND	ND	ND

[3] Datasets were downloaded from NCBI GEO or obtained from Chin et al. (Chin, et al. 2006) and analyzed for gene expression differences between classes based on ER status and molecular subtype (Student's t-test)

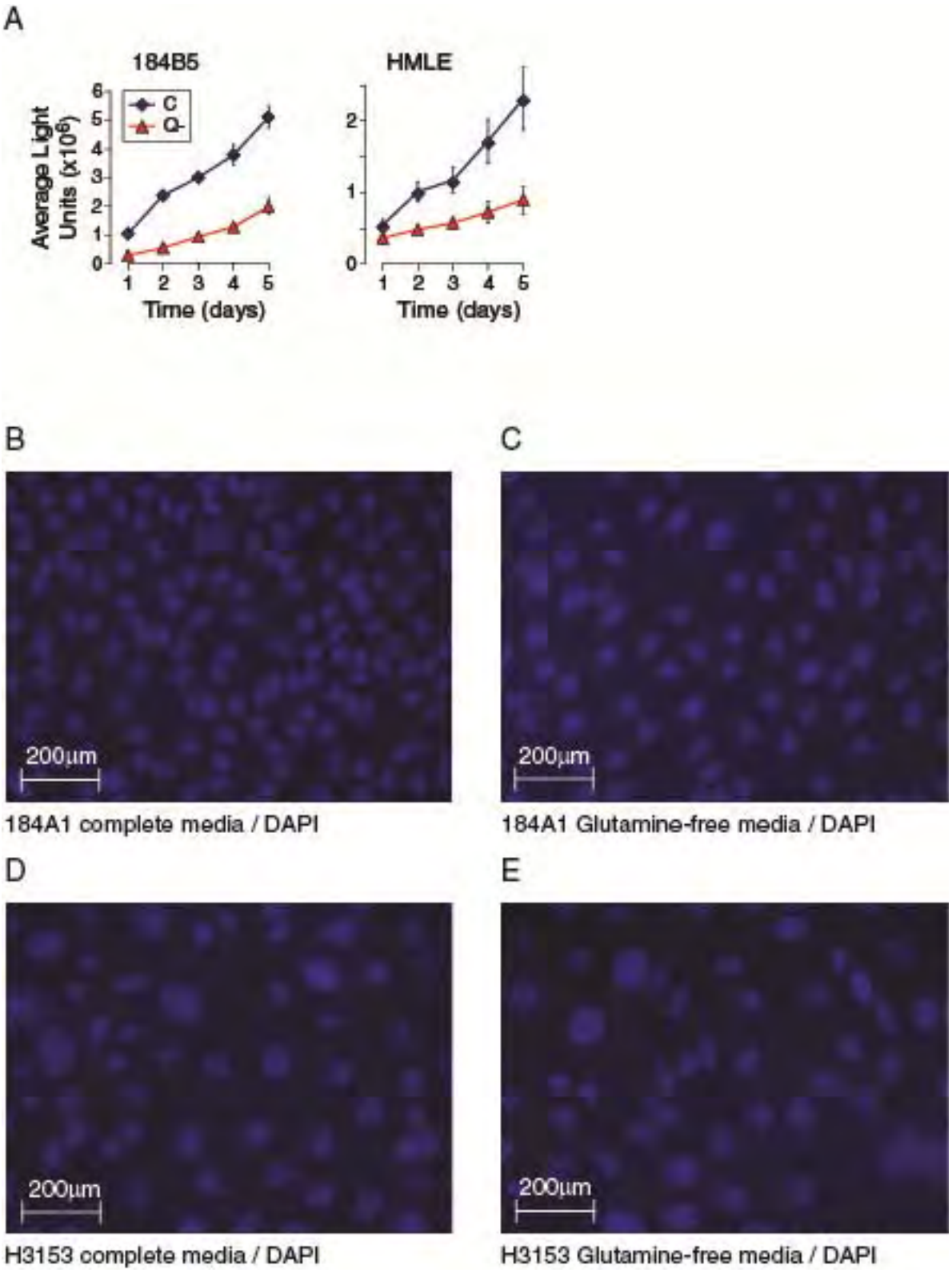

Figure S2, related to Figure 2. Non-Tumorigenic Cells Adapt to Glutamine Restriction by Slowing Culture Expansion

(A) Growth curves of two additional non-tumorigenic cell lines (184B5, HMLE); C, complete media; Q-, glutamine-free media. Icons represent mean values; error bars, standard deviations. (B-E) Regular nuclear morphology of glutamine free and complete media cultures (DAPI stain). (B and C) 184A1 non-tumorigenic cells; (D and E) H3153, a similarly-sensitive TNBC line.

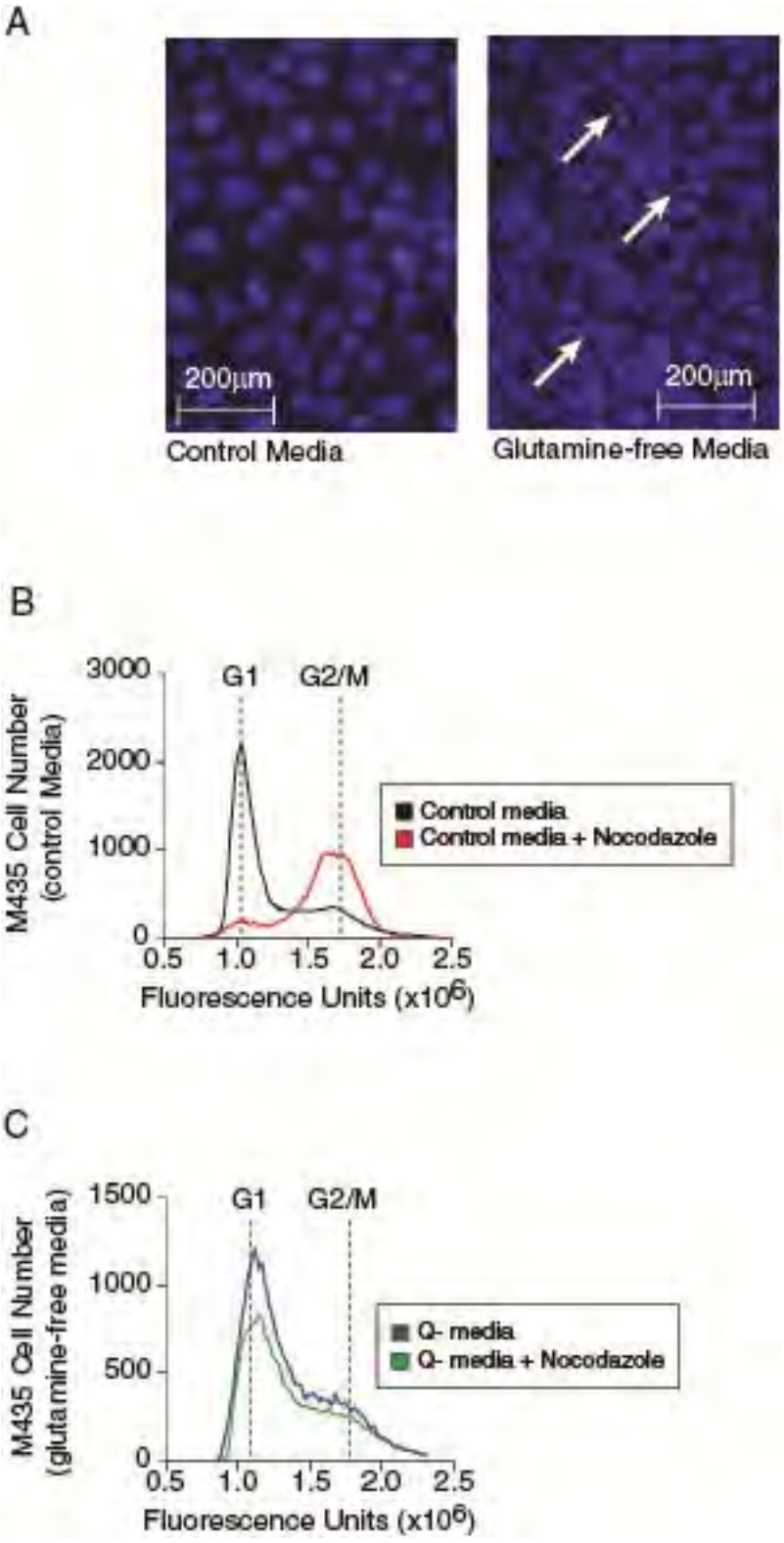

Figure S3, related to Figure 3. Glutamine Restriction Induces S-Phase Stalling and Apoptosis in Group C Carcinomas

Icon codes in figure keys. (A) Nuclear morphology (DAPI stain) of a representative group C TNBC line grown in (left) control media vs. (right) glutamine free media, arrows at apoptotic figures. (B) Example cell cycle profiles of a Group C TNBC line cultured 5 days in complete media with and without 18 hours nocodazole treatment (red vs. black curves); (C) Example cell cycle profiles of a Group C TNBC line cultured 5 days in glutamine-free media without and with 18 hours nocodazole treatment (blue vs green curves)

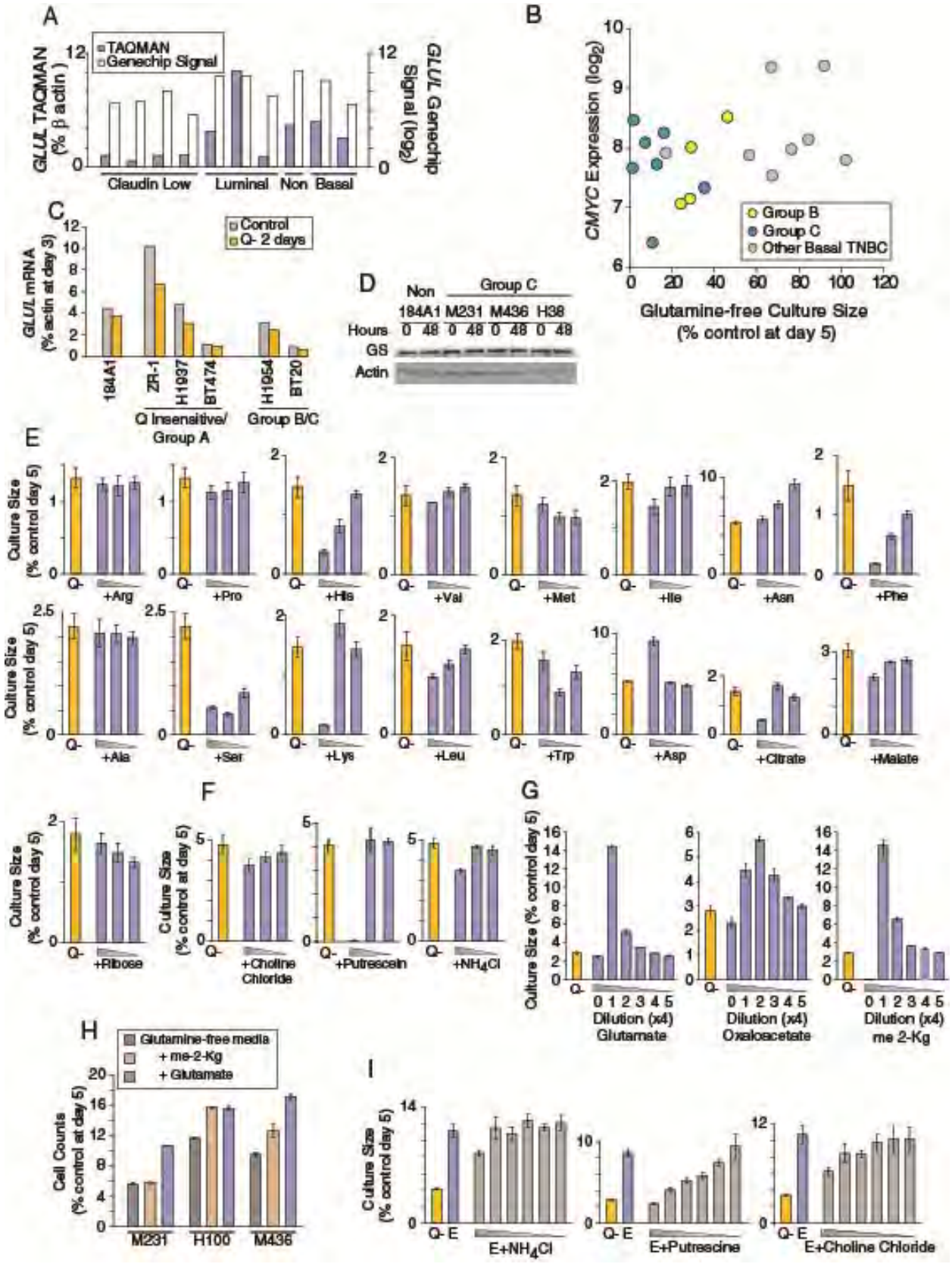

Figure S4, related to Figure 4. Glutamine is an irreplaceable nutrient for some TNBC

Icon codes in figure keys. Icons represent mean values +/-SD. (A) TAQMAN validation of relative *GLUL* Genechip signals for representative cells in our panel. (B) *cMYC* genechip hybridization signal (y-axis) versus glutamine-free culture sizes, derived from Figure 2A. (C) *GLUL* mRNA is not induced upon glutamine restriction; Q insensitive, basal TNBC with smaller glutamine-restricted proliferative defects than the non-tumorigenic cell lines; paired bars represent mRNA measurements (TAQMAN) in individual cell lines; Control, control media; Q-, glutamine-free media (see also Figure 4E). (D) Glutamine synthetase protein levels are not substantially altered in response to 48 hours of glutamine restriction; non, non tumorigenic exemplar 184A1. (E-H) Proliferative analysis of alternate nutrient additions; values normalized to control media population sizes; Icons represent mean values; error bars, standard deviations. (E) Yellow bar, Q-, glutamine free media alone; blue bars, glutamine free media plus 20mM alternate nutrient and 2 serial 4X dilutions shown; standard three letter abbreviations used for amino acids. (F) Titrations of amino group sources does not restore culture expansion, icon codes and conditions per part E. (G, H) Nutrients that marginally increase glutamine-free culture sizes; me 2-KG, dimethyl 2-ketoglutarate. (G) ATP-based cell titer assay using M436; icon codes and conditions per part E. (H) Direct cell counts (Accuri) in 3 Group C cell lines. (I) Glutamate plus titrations of amino group sources do not improve culture expansion over glutamate alone in glutamine-free media; yellow bar, Q-, glutamine free media alone; E, glutamate in glutamine-free media; gray bars, various amino group sources with glutamate in glutamine-free media; dilutions are 4X from 20mM.

Table S4, related to Figure 4. Class Associations of *GLUL* in Expression Datasets Derived from Primary Clinical Tumor Samples[4]				
Gene Set ID	**Association tested**	***GLUL* 200648_s_at**	***GLUL* 217202_s_at**	***GLUL* 215001_s_at**
GSE 1561	ER (ER+) Subtype (Luminal)	0.171 / -1.36 0.828 / -1.10	0.149 / -1.30 0.830 / -1.09	0.741 / 1.04 0.196 / 1.15
GSE 2034	ER (ER+)	0.024 / 1.30	0.024 / 1.16	1.3e-15 / 1.81
GSE 20271	ER (ER+)	2.3e-6 / 2.13	9.4e-5 / 1.65	4.0e-8 / 1.93
GSE 23988	ER (ER+)	2.1e-4 / 2.66	0.004 / 1.92	4.7e-6 / 2.20
GSE 4922	ER (ER+)	9.2e-4 / 1.87	5.7e-4 / 1.92	1.0e-6 / 1.61
GSE 1456	Subtype (Luminal)	1.0e-8 / 4.52	3.9e-7 / 3.64	4.9e-10 / 2.63
GSE 7390	ER (ER+)	5.4e-6 / 1.95	1.8e-6 / 1.99	1.7e-9 / 1.75
Chin 2006	ER (ER+)	0.005 / 2.09	0.004 / 2.44	8.6e-7 / 1.73
Chin 2006	Subtype (eucl) (Luminal)	2.1e-4 / 2.82	8.3e-5 / 3.49	2.7e-10 / 2.36
Chin 2006	Subtype (corr) (Luminal)	2.7e-4 / 2.79	1.3e-4 / 3.47	5.6e-10 / 2.31

[4] Datasets were downloaded from NCBI GEO or obtained from Chin et al. (Chin, et al. 2006) and analyzed for gene expression differences between classes based on ER status or molecular subtype: p value (t-test) / fold change, where ratio of average marker expression in ER+/luminal vs. ER-/basal samples in raw expression data (>1 means up-regulation in ER+/luminal, and <-1 means up-regulation in ER-/basal).

Table S5, related to Figure 4. Myc Association Statistics			
Probeset ID	**Myc Family Member / Transcriptional Target Gene**	**t-test Group C vs all Basal + Claudin low, p =**	**t-test Group B+C vs all Basal + Claudin Low, p =**
202922_at	GCLC, glutamate-cysteine ligase, catalytic subunit	0.680732996	0.285144004
202923_s_at	GCLC, glutamate-cysteine ligase, catalytic subunit	0.930452219	0.232623985
203925_at	GCLM, glutamate-cysteine ligase, modifier subunit	0.744924053	0.992793651
221510_s_at	GLS, glutaminase	0.07184016	0.30721294
203157_s_at	GLS, glutaminase	0.038305794	0.066323391
203158_s_at	GLS, glutaminase	0.158391485	0.482694785
203159_at	GLS, glutaminase	0.114072714	0.225283679
205531_s_at	GLS2, glutaminase 2 (liver, mitochondrial)	0.074431839	0.088951816
200648_s_at	GLUL, glutamate-ammonia ligase (glutamine synthase)	0.259776929	0.026125116
215001_s_at	GLUL, glutamate-ammonia ligase (glutamine synthase)	0.792003217	0.17200119
217202_s_at	GLUL, glutamate-ammonia ligase (glutamine synthase)	0.245547385	0.053102733
200650_s_at	LDHA, lactate dehydrogenase A	0.266049864	0.082323534
208403_x_at	MAX, MYC associated factor X	0.981466482	0.951836406
209331_s_at	MAX, MYC associated factor X	0.249051824	0.604375051
209332_s_at	MAX, MYC associated factor X	0.116828225	0.070735325
210734_x_at	MAX, MYC associated factor X	0.762960743	0.835511118
203159_at	GLS, glutaminase	0.114072714	0.225283679
214108_at	MAX, MYC associated factor X	0.749550292	0.414116063
207824_s_at	MAZ, MYC-associated zinc finger protein (purine-binding transcription factor)	0.003248803	0.000688372
212064_x_at	MAZ, MYC-associated zinc finger protein (purine-binding transcription factor)	0.006013447	0.036746352
213188_s_at	MINA, MYC induced nuclear antigen	0.422365219	0.389165846
213189_at	MINA, MYC induced nuclear antigen	0.272299316	0.347385343
202431_s_at	MYC, v-myc myelocytomatosis viral oncogene homolog (avian)	0.15501392	0.068167919

Table S5 (cont'd). Myc Association Statistics[5]			
Probeset ID	**Myc Family Member / Transcriptional Target Gene**	**t-test Group C vs all Basal + Claudin low, p =**	**t-test Group B+C vs all Basal + Claudin Low, p =**
203359_s_at	MYCBP, c-myc binding protein	0.747532179	0.141452857
203360_s_at	MYCBP, c-myc binding protein	0.459129501	0.181826356
203361_s_at	MYCBP, c-myc binding protein	0.673391404	0.456707435
201959_s_at	MYCBP2, MYC binding protein 2	0.56877653	0.116142118
201960_s_at	MYCBP2, MYC binding protein 2	0.843906145	0.156008882
209757_s_at	MYCN, v-myc myelocytomatosis viral related oncogene, neuroblastoma derived (avian)	0.318485559	0.234655027
214787_at	MYCPBP, c-myc promoter binding protein	0.600841503	0.039313472
203964_at	NMI, N-myc (and STAT) interactor	0.586342711	0.199606276
201599_at	OAT, ornithine aminotransferase (gyrate atrophy)	0.324024156	0.233368527
204243_at	RLF, rearranged L-myc fusion sequence	0.673422221	0.199249805
208916_at	SLC1A5, solute carrier family 1 (neutral amino acid transporter), member 5	0.632444253	0.968534998
218237_s_at	SLC38A1, solute carrier family 38, member 1	0.2669149	0.02960135
218041_x_at	SLC38A2, solute carrier family 38, member 2	0.635279484	0.554865205
220924_s_at	SLC38A2, solute carrier family 38, member 2	0.671218493	0.525109732
207528_s_at	SLC7A11, solute carrier family 7, (cationic amino acid transporter, y+ system) member 11	0.072142142	0.016771364
201195_s_at	SLC7A5, solute carrier family 7 (cationic amino acid transporter, y+ system), member 5	0.91245638	0.347283019

[5]A summary of statistical analyses (t-tests) comparing expression levels of MYC, MYC family members, and various Myc transcriptional targets in the auxotrophic samples (Groups B and C) versus other basal and claudin low samples. Expression values from Affymetrix U133A genechip hybridization signals

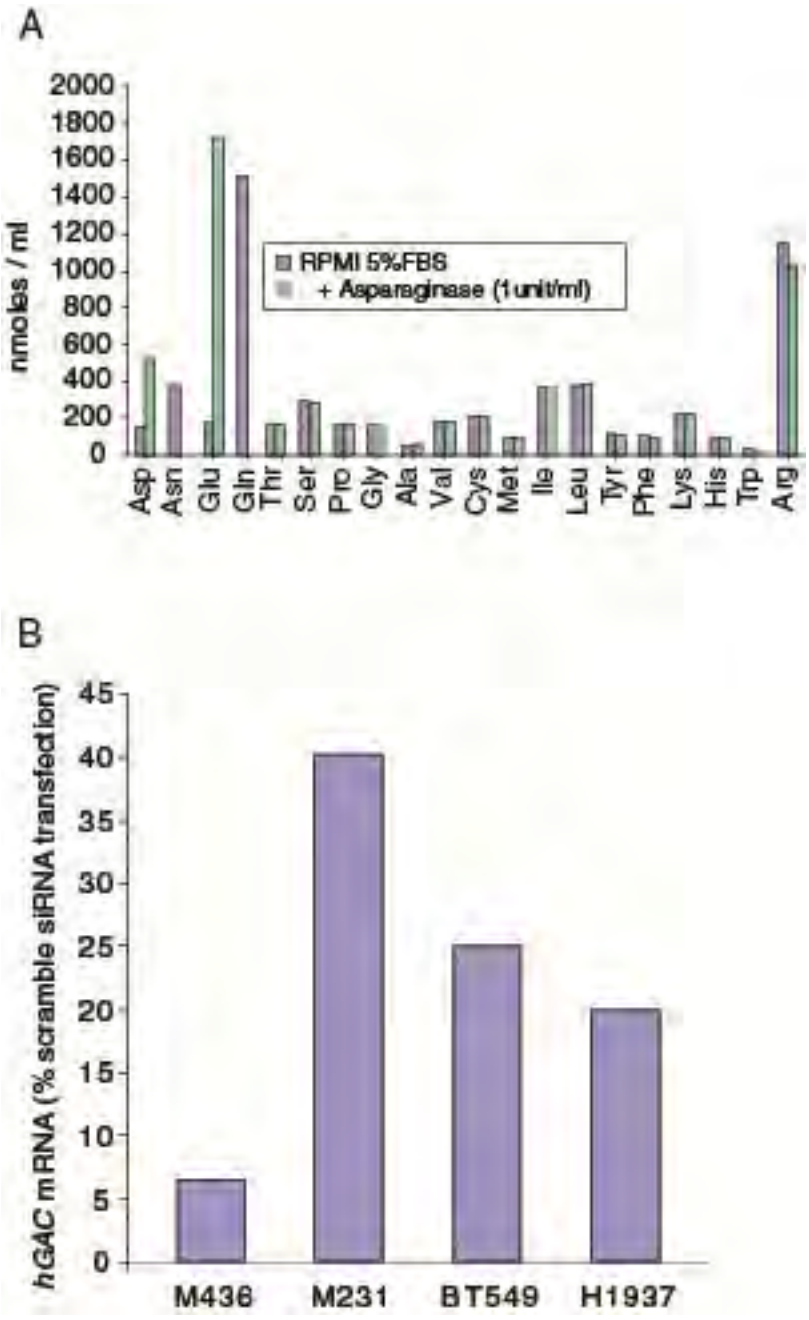

Figure S5, related to Figure 5. Glutamine Auxotrophy Presents Therapeutic Opportunity

(A) Amino acid analysis of RPMI culture media treated with and with out Asparaginase (1u/ml); standard 3-letter amino acid abbreviations used, analysis by HPLC. (B) Efficiency of *hGAC* siRNA-mediated mRNA knockdown in 4 exemplar cell lines, values normalized to *hGAC* message levels in each cell line transfected with a negative control siRNA. Corresponding proliferative defects illustrated in Figure 5H.

Table S6, related to Figure 5. Class Associations of Glutamine Transporter Probeset IDs in Expression Datasets Derived from Primary Clinical Tumor Samples[6]							
Gene Set ID	**Association tested**	***ASCT2* 208916_at**	***SLC38A1* 218237_s_at**	***SLC38A2* 220924_s_at**	***SLC38A2* 218041_x_at**	***SLC7A5* 201195_s_at**	***SLC3A2* 200924_s_at**
GSE1561	ER (ER+)	0.339 / -1.07	0.318 / 1.19	0.051 / 1.27	0.038 / 1.29	4.5e-6 / -2.64	0.765 / -1.00
	Subtype (Luminal)	0.286 / 1.09	0.003 / 2.35	0.014 / 1.37	0.015 / 1.37	3.6e-5 / -2.12	0.407 / 1.18
GSE2034	ER (ER+)	0.016 / -1.16	0.018 / 1.24	0.519 / 1.06	0.551 / 1.06	1.1e-15 / -2.52	0.019 / -1.14
GSE20271	ER (ER+)	0.337 / -1.02	0.006 / 1.56	0.008 / 1.32	0.003 / 1.35	1.6e-4 / -1.64	0.539 / -1.02
GSE23988	ER (ER+)	0.248 / 1.11	2.3e-5 / 2.91	9.6e-6 / 2.05	7.4e-6 / 2.18	0.054 / -1.18	0.480 / 1.12
GSE4922	ER (ER+)	0.267 / -1.05	0.042 / 1.41	0.902 / 1.07	0.937 / 1.05	1.91e-12 / -3.24	0.699 / 1.06
GSE1456	Subtype (Luminal)	0.145 / 1.15	0.013 / 1.91	0.295 / -1.14	0.411 / -1.12	1.7e-5 / -2.84	0.868 / -1.00
GSE7390	ER (ER+)	3.4e-5 / -1.31	0.021 / 1.03	0.695 / -1.02	0.519 / -1.05	1.1e-15 / -3.08	0.005 / -1.15
Chin 2006	ER (ER+)	0.192 / -1.03	0.132 / 1.43	0.180 / 1.21	0.335 / 1.19	1.1e-6 / -2.30	0.175 / 1.12
Chin 2006	Subtype (eucl) (Luminal)	0.556 / 1.05	0.008 / 2.23	0.023 / 1.36	0.036 / 1.34	1.1e-7 / -2.57	0.878 / 1.29
Chin 2006	Subtype (corr) (Luminal)	0.475 / 1.03	0.014 / 2.19	0.052 / 1.30	0.074 / 1.28	1.8e-7 / -2.38	0.769 / 1.30

[6]Datasets were downloaded from NCBI GEO or obtained from Chin et al. (Chin, et al. 2006) and analyzed for gene expression differences between classes based on ER status or molecular subtype: p value (t-test) / fold change, where ratio of average marker expression in ER+/luminal vs. ER-/basal samples in raw expression data (>1 means up-regulation in ER+/luminal, and <-1 means up-regulation in ER-/basal).

Table S7, related to Figure 5. Metabolomics Results[7]							
13C label Source / Time	**Metabolite analyzed (+X denotes number of ^{13}Carbons)**						
	Asp+0	**Asp+1**	**Asp+2**	**Asp+3**	**Asp+4**		
12 hr 13C glutamine	25.1%	10.6%	18.0%	8.2%	38.1%		
12 hr 13C glutamine	25.5%	10.3%	16.0%	9.7%	38.5%		
6 hr 13C glutamine	28.7%	8.7%	15.7%	9.0%	37.8%		
average	**26.5%**	**9.9%**	**16.6%**	**9.0%**	**38.1%**		
standard deviation	**2.0%**	**1.0%**	**1.2%**	**0.8%**	**0.3%**		
	Citrate+0	**Citrate+1**	**Citrate+2**	**Citrate+3**	**Citrate+4**	**Citrate+5**	**Citrate+6**
12 hr 13C glutamine	27.4%	10.6%	18.8%	8.8%	31.8%	2.6%	0%
12 hr 13C glutamine	29.6%	10.8%	18.7%	5.6%	28.9%	6.5%	0%
6 hr 13C glutamine	31.6%	7.3%	14.4%	11.6%	33.1%	2.0%	0%
average	**29.5%**	**9.6%**	**17.3%**	**8.7%**	**31.3%**	**3.7%**	**0.0%**
standard deviation	**2.1%**	**2.0%**	**2.5%**	**3.0%**	**2.2%**	**2.4%**	**0.0%**
	Glu+0	**Glu+1**	**Glu+2**	**Glu+3**	**Glu+4**	**Glu+5**	
12 hr 13C glutamine	31.2%	4.8%	2.4%	16.0%	3.2%	42.3%	
12 hr 13C glutamine	27.0%	4.8%	3.5%	11.6%	7.3%	45.8%	
6 hr 13C glutamine	24.7%	5.3%	4.7%	14.5%	1.9%	48.9%	
average	**27.6%**	**5.0%**	**3.5%**	**14.0%**	**4.1%**	**45.7%**	
standard deviation	**3.3%**	**0.3%**	**1.1%**	**2.3%**	**2.9%**	**3.3%**	
	Gln+0	**Gln+1**	**Gln+2**	**Gln+3**	**Gln+4**	**Gln+5**	
12 hr 13C glutamine	17.8%	5.4%	0.0%	0.0%	4.2%	72.6%	
12 hr 13C glutamine	12.3%	1.5%	0.0%	0.0%	5.0%	81.2%	
6 hr 13C glutamine	10.2%	0.0%	0.1%	0.8%	3.5%	85.3%	
average	**13.4%**	**2.3%**	**0.0%**	**0.3%**	**4.2%**	**79.7%**	
standard deviation	**4.0%**	**2.8%**	**0.1%**	**0.5%**	**0.7%**	**6.5%**	
	Malate+0	**Malate+1**	**Malate+2**	**Malate+3**	**Malate+4**		
12 hr 13C glutamine	26.1%	11.4%	19.9%	6.2%	36.4%		
12 hr 13C glutamine	24.6%	10.5%	19.4%	6.6%	38.8%		
6 hr 13C glutamine	26.0%	9.4%	15.5%	9.5%	39.6%		
average	25.6%	10.4%	18.3%	7.4%	38.3%		
standard deviation	0.8%	1.0%	2.4%	1.8%	1.6%		

[7] Incorporation of ^{13}C-carbon from exposure to ambient ^{13}C-5-glutamine by various metabolites as indicated in gray rows, expressed as percent total metabolite pool analyzed. Columns report percent per number of labeled carbons in each substrate pool.

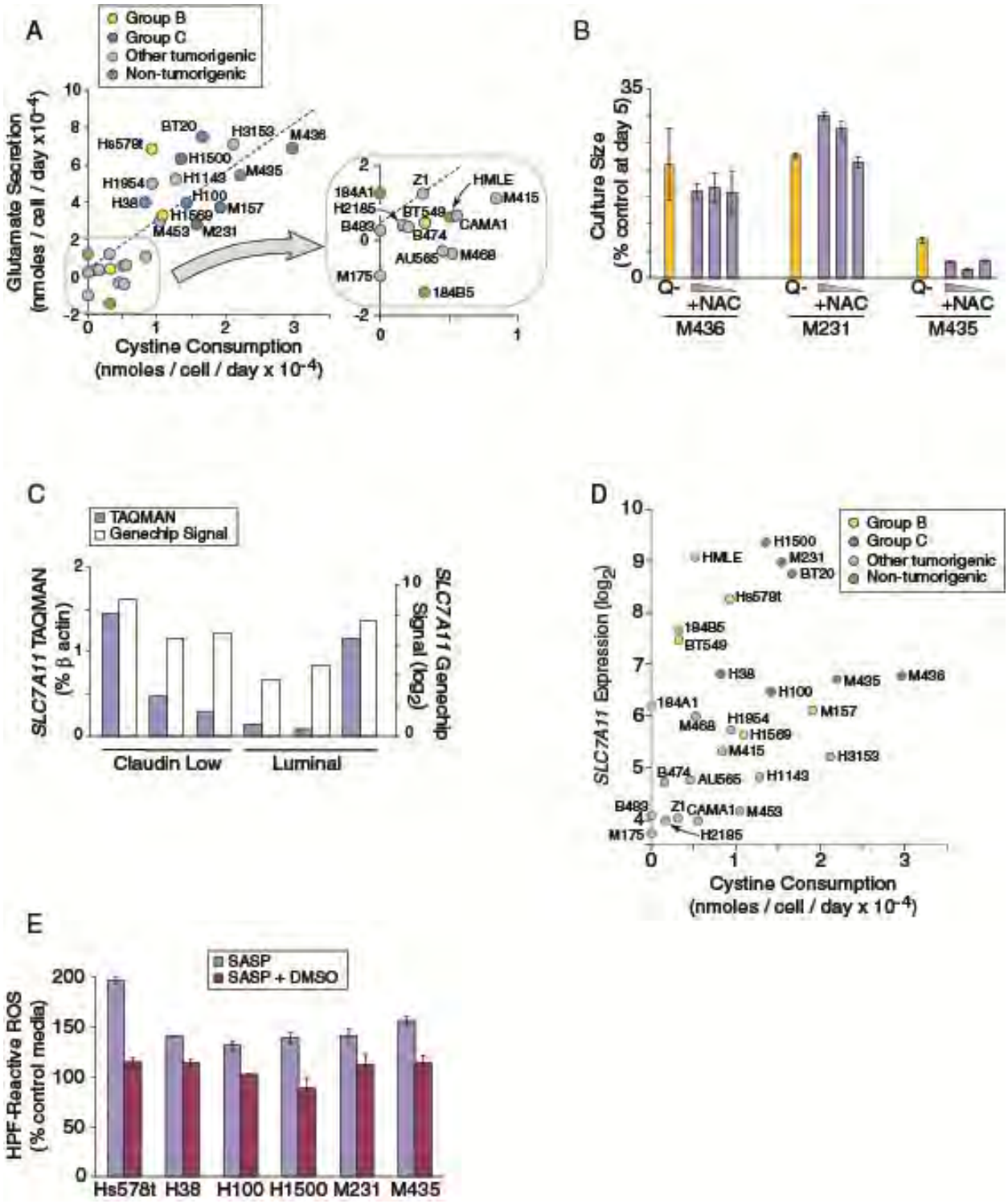

Figure S6, Related to Figure 6. xCT-Mediated Cystine Transport Raises Free Radical Levels in TNBC

Icon codes in figure keys. Icons represent mean values+/-SD. (A) Duplicate of Figure 6A color coded by glutamine restriction group membership illustrating cystine consumption vs. glutamate secretion, derived from HPLC analysis of culture supernatants. (B) N-acetylcystine does not substantially restore culture expansion in the absence of glutamine; 3 exemplar Group C TNBC samples shown; values normalized to parallel cultures in control media; Q-, glutamine free media; NAC, 4-fold titrations of N-acetylcystine from 20mM in glutamine-free media. (C) TAQMAN validation of relative *SLC7A11* Affymetrix genechip signals for representative cells in our panel. (D) Relationship between *SLC7A11* Genechip hybridization signals and cystine consumption, icons coded by glutamine restriction group membership. See figure 6C for coding by molecular subtype. (E) Quantitation of HPF (hydroxyphenylfluorescine) reactivity in response to 300μM SASP treatment, derived from FACS analysis (FL-1 channel detection). Parallel cultures using SASP + 2% DMSO exhibit reduced HPF signal, indicating the specific reduction in hydroxyl radicals (maroon bars).

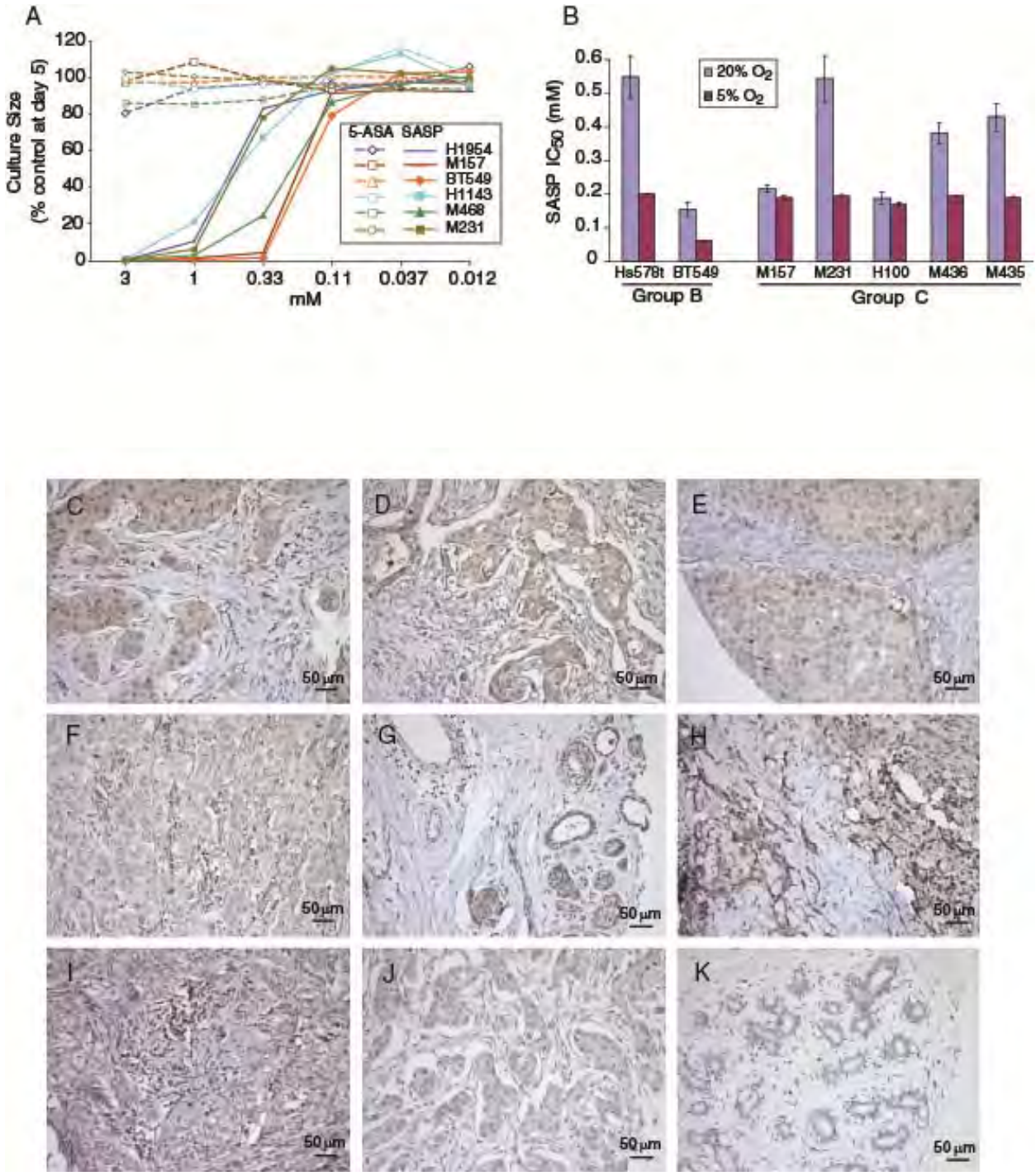

Figure S7, related to Figure 7. The xCT Transporter is Expressed in Breast Tumors *in vivo*, and is Therapeutically Inhibited by Sulfasalazine

Icons represent mean values+/-SD. (A) Comparison of SASP and the anti-inflammatory cleavage product 5-ASA for growth attenuation in 6 exemplar basal and claudin low TNBC. Identical titrations shown, values expressed as % of parallel control media cultures. Open icons

and dotted lines, 5-ASA treatment; closed icons and solid lines, 300μM SASP treatment. B) Comparison of SASP sensitivity in ambient (20%) oxygen (blue bars); vs. tissue normoxia (5% O_2), maroon bars. (C-K) Staining results showing xCT expression in paraffin sections of anonymous TNBC breast tumors; blue, Hematoxylin (nuclei); brown, horseradish peroxidase (specific anti-xCT stain). (C-I) Images of tumors counted as strong xCT staining. (J) Images of tumor counted as light xCT stain. (K) Normal breast section, with infrequent xCT positive stromal cells.

SUPPLEMENTAL EXPERIMENTAL PROCEDURES

Purification of Normal Mammary Epithelial Cells

Purified from 3 distinct reduction mammoplasties as previously described, collected under IRB approval (Allinen et al., 2004). Briefly, tissue was minced, digested with collagenase I (Sigma C0130) and hyaluronidase (Sigma H3506) 1-2 hrs/37C, washed, filtered through graded pore sized strainers (Tetko, 03-500-47, 03-250-50 and 03-20-14, Fisher 08-771-19 and 08-771-1) to harvest organoids (filter tops). These were trypsinized (5 min/ 37C), filtered (100μm, 40μm, and 20μm mesh), single cell flow through put on Percoll gradients to remove debris and erythrocytes (Percoll-Pharmacia 17-0891-01). Luminal epithelia were purified via anti-BerEP4-conjugated magnetic bead adherence, basal/myoepithelia by anti-CD10-conjugated beads. Cells were immediately frozen on dry ice. Samples were at least 95% pure by PCR.

Pleural Effusion Tumor Cell Purification and Analysis

Patient permission was obtained under IRB approval. Cells were purified by centrifugation, red blood cells lysed, and remainders frozen in aliquots in 10% DMSO/ 90% FBS/ liquid nitrogen. Tumor abundance, purity, and phenotype were determined by immune fluorescence on cytospin samples using markers of carcinomas, mesothelia, lymphocytes, and endothelia. Cytospins were fixed/permeabilized in 1% paraformaldehyde/ 0.1% Triton-X 100 or 100% methanol. Antibodies: BD Transduction Labs: Cytokeratin 8, CAM 5.2,1:3; MUC1, 555925; CD44, 550392; Moesin, 610401; E-cadherin, 610181; VE-cadherin, 555289. Zymed: Mesothelin,35-4200; Calretinin, 18-0291; OB-cadherin, 32-1700; N-cadherin, 33-3900. Neomarkers: Vimentin, MS-129-PO; P-cadherin, MS-1741-S0; CD10, MS-973-PO; BerEP4, MS-1851-P0. Novocastra Cytokeratin 8, RTU-CK8-TS1; DAKO, Cytokeratin 17, M7046; CHEMICON Cytokeratin 5/14, CBL267; Sigma Smooth Muscle Actin, F3777; Santa Cruz Biotechnology Estrogen Receptor, SC-8002. Samples with large tumor clumps that excluded contaminating cells were re-

suspended in warm DMEM/10% FBS, applied to 30μm MACS Pre-Separation Filters (Milteny Biotech 130-041-407), filter-top material (tumor clumps) washed 5 times with fresh media on the filter, an aliquot methanol fixed to gauge purity, and the remainder re-suspended in lysis buffer (XB, NuGEN), and frozen on dry ice. SUM86PE: 85% tumor cells, 10% medium sized vimentin$^+$ cells, remainder small vimentin positive lymphocytes. SUM87PE: Homogenous large epithelial clumps, 0.7% small vimentin positive lymphocytes. SUM 153 PE: Homogenous tumor clumps, 2.6% lymphocytes.

Dataset Generation

RNA was prepared (PicoPure RNA Isolation Kit 0204, Arcturus) from samples described above, from 4 non-tumorigenic human mammary epithelial cell (HMEC)-derived cell lines: (184A1, 184B5, HMLE, HMLE-PR) (Stampfer, Hallowes et al. 1980; Elenbaas, Spirio et al. 2001), and 10 carcinoma-derived cell lines previously determined by Neve, et. al. (Neve, 2006; "Neve dataset"). Quality was assessed (Agilent Technologies 2100 Bioanalyzer). Labeled cDNA was prepared from 50 ng total RNA (Ovation Biotin RNA Amplification and Labeling System, NuGEN) per manufacturers' instructions, and hybridized to Affymetrix U133A GeneChips using standard procedures developed and performed by the David J. Gladstone Institute Genomics Core, UCSF. Affymetrix image files were normalized (RMA, (Irizarry et al., 2003)), and the resultant $\log_2$ values used to produce the dataset Timmerman_pico. Datasets merge: The mean hybridization signal for each probeset ID across all samples in the Neve dataset (jmean), and the mean hybridization signal for each probeset ID across the 10 breast cancer derived cell lines (CDL) in the Timmerman_pico dataset were determined (lmean). Mean value differences between the Timmerman_pico and Neve datasets were calculated for each probeset ID (jmean-lmean), and added to each sample in the Timmerman_pico dataset. Values for the 10 duplicated CDL in the resulting merged dataset (Timmerman_merge) were examined before all subsequent analyses to verify that signal hybridization alterations in the merged dataset were

not due to sample preparation or dataset normalization. Duplicate samples in the Timmerman_merge dataset derived from the Timmerman_pico source were then removed before all statistical and bioinformatics-based dataset analyses. Cluster and Treeview software were used (Eisen et al., 1998) to visualize group relationships.

Significance Analyses

Several two class unpaired analyses using Significance Analysis for Microarray EXCEL spreadsheet add in (Tusher et al., 2001) were performed. The first contrasted the purified normal and non-tumorigenic, HMEC-derived samples (the N/I class) against the Carcinoma-derived lines (CDL) plus the purified pleural effusion tumors (PE) samples (the CDL/PE class). We identified 2887 significant Probeset IDs with a median of 0.41 Probeset IDs falsely called; 1631 positively associated and 1256 negatively associated with the CDL/PE (ie: positively associated with the N/I class). More than 28.4% versus 8.0% of all transcripts associated with the CDL/PE versus the N/I group encode molecules involved in intracellular metabolism and other mitochondrial-specific functions. To identify CDL subtype-specific metabolic transcripts, all Probeset IDs associated with metabolic GO descriptions were selected from the Timmerman_merge dataset, (2003 Probeset IDs in total) and two additional significance analyses were performed, pitting the luminal CDL/PE (the "LUMINAL analysis") and then the basal/mesenchymal CDL (the "BASAL/MES analysis") against all other samples. About 360/760 metabolic probeset IDs identified in the N/I versus CDL/PE significance analysis were-re identified in these two latter analyses, suggesting that almost half (47%) of transcripts identified as CDL/PE-associated are in fact on this list based on alterations in only a subset of the samples, and further strengthening the impression of strong metabolic differences between the luminal and basal/mesenchymal CDL. At highest stringency, about 202 novel probeset IDs with positive, and 31 with negative luminal CDL/PE expression bias were also identified. Similarly, at highest stringency 142 new Probeset IDs with positive basal/mesenchymal CDL

subset expression bias were uniquely identified. Essentially all probeset IDs negatively associated with the basal/mesenchymal CDL class were also positively associated with the luminal CDL/PE in the luminal analysis above (77/86); three remaining probeset IDs were previously positively associated with the N/I clade, providing 6 unique Probeset IDs negatively associated with the basal/mesenchymal clade. These significance analyses have highlighted about 760 Probeset IDs which identify molecules involved in intracellular metabolic processes and mitochondrial functions that are expressed differentially between these 4 classes of samples: the N/I, the CDL/PE, the luminal CDL/PE, and the basal/mesenchymal CDL.

TP53 Analysis

Using the IARC TP53 Database (http://p53.iarc.fr/CellLines.aspx), we found 36 of our cell lines with reliable information on TP53 status. They include 15 luminal, 13 basal, and 8 claudin low samples, 27 with p53 mutations, and 9 wildtype. Of the mutant alleles, 14 have no assessment as to functionality, while the remaining 19 are deemed nonfunctional by various analyses summarized in the database, including protein structure and the ability to transactivate transcription. Of the 36 cell lines, 10 are glutamine sensitive cells (7 Group C and 3 Group B). We did not identify any correlation between p53 status and glutamine dependency. We have included this result in the text.

	p53 Mutant	Deleterious / Nonfunctional (no information)	p53 WT	Total
Luminal	9	8 (1)	6	15
Basal	11	6 (5)	2	13
Cl. Low	7	5 (2)	1	8
Total	27	19 (14)	9	36

	Mutant vs. WT	Nonfunctional vs. All
t-test Group C vs. All p=	8.31E-01	5.81E-01
t-test GroupC+B vs. All p=	6.71E-01	6.97E-01

DAPI Nuclear Stain

Subconfluent cultures were grown on coverslips, paraformaldehyde fixed (2% / 20 min/room temp), and nuclei stained by standard methods (DAPI, Molecular Probes). Nuclear morphology, mitotic frequency, and apoptotic figure assessment was done by manual cell counts of at least 2000 cells/condition.

Quantitative PCR

RNA samples were prepared (Quiagen RNA Mini Kit) and specific primer/probe mixes used (Assay-on-Demand, Applied Biosystems, or a custom designed IDT PrimeTime Mini qPCR Assay specific for the *hGAC* splice variant) to quantify specific message levels (*Taq*Man, Applied Biosystems PRISM 7900). Exemplar cell lines representing low and high expression were selected for each gene analyzed to validate genechip hybridization variation, or for analysis of expression alterations with glutamine restriction.

For Figures S5B, 4E, 4F, 5H6H: 1.5ug total RNA (NucleoSpin RNAII kit, Macherey-Nagel), was reverse transcribed (iScript, Biorad) per manufacturer's directions. Power SYBR (AB) green PCR reactions performed in triplicate, analyzed with the Step One Plus (AB) sequence detection system. Data quantified against a standard curve, normalized to *TBP* (TATA box binding protein). Primers: *hGAC*: 5' GGGAATTCACTTTTGTCACGATC, 5' CTTTCATAGTCCAATGGTCCAAAG; *GLUL*: 5' AAGGTGTGTGGAAGAGTTGCC, 5' TGCTCACCATGTCCATTATC; *xCT*: 5' TGCTGGGCTGATTTTATCTTCG, 5' GAAAGGGCAACCATGAAGAGG; *TBP*: 5' CCCGAAACGCCGAATATAATCC, 5' GACTGTTCTTCACTCTTGGCTC.

Western Blot

RIPA extracts were prepared by standard techniques in the presence of protease and phosphatase inhibitors. 20 μg of lysates were resolved on 4-20% polyacrylamide gels, transferred to PVDF membrane, blocked in 5% BSA/TBST 30 minutes, exposed to primary

antibodies overnight/4C in blocking buffer. Specific hybridization was visualized with HRP-conjugated secondary and chemiluminescence (Amersham RPN2106). Antibodies: AMPK, p-AMPK T-172, ACC, p-ACC S-79, cleaved PARP, retinoblastoma, and phosphorylated retinoblastoma (Cell Signaling); glutaminase (Abnova H00002744-M01); glutamine synthase (Santa Cruz sc-9067); beta actin (Sigma). Glutaminase assembly, Figure S1E; M231 extracts were included on each of 6 separate blots, to normalize signal intensities for the assembly in Photoshop. Duplicate M231 lanes were removed after assembly. Signal intensities were scored as none=1, light=2, strong=3. Pairs of sibling cell lines (asterisks) are counted as one independent isolate (AU565 and SKBR3, MCF7 and LY2).

Culture Expansion Assays

Assays were performed at least 3 times in triplicate, in 96-well format. Relative cell number determined (Cell Titer Glow, Promega), verified by microscopy. Averages reported +/-SD.96-well format triplicate cultures at 1-4X10^4/ml or, confluent 1-4X10^5 /ml, with control, glutamine deficient,(GIBCO 21870, 11960), or 3 or 4-fold serial drug/ nutrient dilutions for 5 days/37^{o}C/5%$CO_{2,}$. Highest concentrations: Asparaginase 100 units/ml, DON 5mM, Sulfasalazine 3mM, N-acetylcysteine 10 mM, 5-ASA 3mM, Carboplatin 100μg/ml, Doxorubicin 150ng/ml, Paclitaxel 1.7 mg/ml. Cell cycle, direct cell counts, glucose uptake, Annexin V, ROS detection and siRNA used larger format cultures.

Doubling Times

Cell numbers in triplicate cultures determined by particle counter (Coulter), ATP levels (Cell-Titer Glow, Promega), or trypan blue exclusion. Growth curve calculations used standard techniques.

Annexin V / Cell Death Assay

FACSCalibur (Becton Dickinson) or C6 Flow Cytometer (Accuri). 30,000 cells in triplicate analyzed, mean fluorescence values reported. Annexin V-FITC (Southern Biotechnology 10038-02) and TOTO3 (Molecular Probes T3604), or Propidium Iodide (PI; Molecular Probes, P1304MP) used per manufacturer's protocol. Percent Annexin V positive, PI negative reported.

Cell Cycle

Cultures +/- 18 hrs 100-200nM nocodazole were 70% ethanol fixed, propidium iodide and RNAse (5ug/ml) stained using standard techniques. 30,000-100,000 cells were analyzed in triplicate. Cell cycle curve fitting and cell cycle fraction calculations by FLOJO curve fitting software (Tree Star, Inc.).

Cell Counts

Live cell numbers in 30μl determined in triplicate using the C6 Flow Cytometer (Accuri). Manual counts used trypan blue exclusion, in triplicate.

SUPPLEMENTAL REFERENCES

Allinen, M., Beroukhim, R., Cai, L., Brennan, C., Lahti-Domenici, J., Huang, H., Porter, D., Hu, M., Chin, L., Richardson, A., et al. (2004). Molecular characterization of the tumor microenvironment in breast cancer. Cancer Cell 6, 17-32.

Elenbaas, B., Spirio, L., Koerner, F., Fleming, M. D., Zimonjic, D. B., Donaher, J. L., Popescu, N. C., Hahn, W. C., and Weinberg, R. A. (2001). Human breast cancer cells generated by oncogenic transformation of primary mammary epithelial cells. Genes Dev 15, 50-65.

Stampfer, M., Hallowes, R. C., and Hackett, A. J. (1980). Growth of normal human mammary cells in culture. In Vitro 16, 415-425.